Geophys. J. Int. (2004) **157,** 87–104 doi: 10.1111/j.1365-246X.2003.02164.x

Return to Black Mountain: palaeomagnetic reassessment of the Chatsworth and Ninmaroo formations, western Queensland, Australia

Kari L. Anderson,[1] Mark A. Lackie,[1] David A. Clark[2] and Phil W. Schmidt[2]

[1] *Department of Earth and Planetary Sciences, Macquarie University, Sydney NSW* 2109, *Australia*
[2] *CSIRO Division of Exploration and Mining, North Ryde NSW* 2113, *Australia*

Accepted 2003 October 20. Received 2003 August 11; in original form 2002 September 4

SUMMARY

Palaeomagnetic results from late Middle Cambrian–Early Ordovician carbonate sequences sampled at Black Mountain (Mt Unbunmaroo), Mt Datson and near Chatsworth Station (south-eastern Georgina Basin) are presented. A palaeomagnetic reassessment of these carbonates was designed in an effort to constrain regional magnetization ages as results from an earlier study, conducted at Mt Unbunmaroo, play a pivotal role in a proposed Cambrian inertial interchange true polar wander (IITPW) event. Remanent magnetizations within these carbonates were found to be variably developed with most specimens displaying two of the five isolated components. Component PF, for which goethite is the identified remanence carrier, is thought to reflect a chemical remanent magnetization of recent origin. Component TR, held by haematite, has a palaeomagnetic pole consistent with the Tertiary segment of Australia's apparent polar wander path (APWP) and most probably was acquired as a consequence of prolonged weathering during this period. The A component has a palaeomagnetic pole at 54.7°S, 262.3°E ($dp = 2.3°$, $dm = 4.5°$) after unfolding. This direction, constrained by positive fold and reversal test statistics, is consistent with Australia's Early Devonian APWP, perhaps reflecting a remagnetization event associated with the intracratonic Alice Springs Orogeny. A Late Ordovician–Early Silurian remanence, component B, is also described; with 100 per cent unfolding the associated palaeopole lies at 8.0°S, 216.8°E ($dp = 2.6°$, $dm = 5.1°$). A third Palaeozoic, and presumed primary or early diagenetic, component, C, also passes applied fold and reversal tests and has a palaeomagnetic pole at 48.6°N, 186.0°E ($dp = 2.1°$S, $dm = 4.0°$). This palaeopole is dissimilar from younger magnetizations, is consistent with Cambrian poles from other parts of cratonic Australia and falls within a cluster of Middle–Late Cambrian (515–500 Ma) palaeopoles from other Gondwanan continents. The age attributed to the palaeopole associated with the C component, ∼510 Ma, provides a tight constraint on the younger boundary of the proposed Cambrian IITPW event and its agreement with other Gondwanan palaeopoles is incompatible with the IITPW hypothesis. Components A, B and C are analogous to palaeomagnetic results reported in the earlier investigation of this region, and a comparison of results from the two studies, coupled with rigorous statistical analyses of the new findings, is presented.

Key words: Australia, Cambrian, Gondwana, IITPW, palaeomagnetism, Palaeozoic.

1 INTRODUCTION

In 1997, Kirschvink *et al.* presented evidence to support a large-scale geodynamic event during the Early–Middle Cambrian based, in part, upon palaeomagnetic data acquired from Cambrian–Ordovician carbonates sampled at Mt Unbunmaroo (Black Mountain), western Queensland (Ripperdan & Kirschvink 1992). This event, thought to be recognized by global plate reorganization and large, equal-magnitude true polar wander (TPW) tracks for all major continents, is known as inertial interchange true polar wander (IITPW). The outcomes of the proposed Cambrian IITPW event were, furthermore, postulated to be critically linked to the 'Cambrian Explosion', a boundary marked by the most massive diversification of genera on Earth yet to be documented (e.g. Narbonne *et al.* 1994).

Since the Cambrian IITPW event was first put forward, Evans (1998) has cited evidence of extremely rapid drift rates during the Vendian–Cambrian boundary, a time in which apparent polar wander

⋆E-mail: kari@geophysik.uni-muenchen.de

paths (APWPs) document plate velocities in excess of 60 cm yr^{-1}, to support the fundamental validity of IITPW, albeit at less than the 90° initially suggested. In this modified true polar wander (TPW) scheme (Evans 1998), palaeomagnetic analyses describe multiple discrete episodes of TPW during the Late Neoproterozoic and Early Palaeozoic, arising from long-lived inertial instabilities related to the break-up of the Rodinian supercontinent. Other authors (Mound *et al.* 1999) have offered compelling preliminary correlations of Cambrian sea levels from Australia, Baltica and Laurentia as an independent means of testing for an IITPW event.

Opposition to the proposed IITPW event has also flourished with (sometimes heated) arguments put forward against the IITPW hypothesis (e.g. Meert 1999; Torsvik & Rehnström 2001; Torsvik *et al.* 1998). Evidence disputing a Cambrian IITPW event focuses on data set selections, controversy over polarity options for pre-Middle Palaeozoic palaeopoles and high rates of apparent polar wander arising from enhanced plate motions due to thermal anomalies in the mantle, rather than the geodynamics of IITPW. Furthermore, the applicability of the CO1° remanence, identified as primary or early diagenetic Late Cambrian–Early Ordovician by Ripperdan & Kirschvink (1992), to Australia's Early Palaeozoic APWP is contested, with some authors advocating remagnetization or regional rotations to account for the anomalous location of the CO1° pole on the Early Palaeozoic APWP for Australia (e.g. McElhinny *et al.* 2003; Meert 1999; Torsvik & Van der Voo 2002).

A rigorous examination of Vendian–Ordovician palaeomagnetic data with regard to the possible occurrence of an IITPW event during this period is not the motivation behind this study. Instead, a palaeomagnetic reinvestigation of Cambrian–Ordovician carbonates at Mt Unbunmaroo was carried out to address the controversy surrounding the palaeomagnetic results of Ripperdan & Kirschvink (1992) and the role of these results in the ensuing IITPW proposal (Kirschvink *et al.* 1997). A parallel section at Mt Datson, approximately 45 km southwest of Mt Unbunmaroo, and sites within the Middle–Late Cambrian Chatsworth and Devoncourt Limestones, exposed to the north of Mts Unbunmaroo and Datson, were also sampled to evaluate the nature of regional magnetizations within the eastern Georgina Basin.

2 REGIONAL GEOLOGY

The Georgina Basin is a large (∼325 000 km^2) Late Proterozoic–Early Palaeozoic intracratonic carbonate basin that covers much of western Queensland and the eastern Northern Territory (Fig. 1, inset). This basin, along with many similarly aged structures within the Australian Craton, is thought to have formed in response to the break-up of a large Proterozoic supercontinent (Lodwick & Lindsay 1990). The fragmentation of this supercontinent, probably Rodinia, gave rise to the extensive Neoproterozoic–Early Palaeozoic Centralian Superbasin (Fig. 1, inset) (Veevers 2000). Three episodes of deformation are recorded within the structural elements of the Centralian Superbasin, including basin inversion during the Late Ordovician–Early Silurian (450–440 Ma), disrupting the Larapitine Seaway that previously linked the eastern and western margins of Australia, and two pulses of deformation (Middle Devonian and Middle Carboniferous) related to the protracted development of the intracratonic Alice Springs Orogeny (ASO) (Haines *et al.* 2001; Scheibner & Veevers 2000). Examples of timing constraints placed upon deformation events within the superbasin remnants include 450–440 Ma upper amphibolite mylonite zones within the Harts Range of the eastern Arunta Inlier (Mawby *et al.* 1999), the Emsian–Eiffelian synorogenic Craven Peak Beds within the Toko Syncline (Turner & Young 1987) and uplift and denudation of the Mt Isa Block during the Middle Carboniferous (Spikings *et al.* 1997).

The Georgina Basin constitutes the present-day northeastern remnant of the Centralian Superbasin in what is now the Burke River Structural Belt (BRSB) (Haines *et al.* 2001). Within the southern BRSB, Late Ordovician–Early Silurian deformation led to the development of the Toko Syncline. Thrust faulting in the Early–Middle Devonian placed the south-western margin of the Toko Syncline beneath the Proterozoic Arunta Inlier, with the whole region again folded during the Middle Carboniferous (Haines *et al.* 2001).

Three areas in the eastern Georgina Basin were examined during this investigation. This sampling scheme included two parallel sections within the Cambrian Chatsworth Limestone and the Cambrian–Ordovician Ninmaroo Formation at Mts Unbunmaroo and Datson, supplemented by sites in Cambrian limestones near Chastworth Station (Fig. 1). Around Chatsworth Station, the carbonates were generally medium- to dark-grey or reddish grey limestones and marls with subhorizontal bedding. At Mt Datson, lithologies ranged between fine-grained, dense medium-grey limestones to light-grey and vuggy dolomitic beds. Beds at Mt Datson were uniformly tilted at about 45°. Units at Mt Unbunmaroo were light grey in colour with dips ranging from subhorizontal to ≤20°. Field notes and laboratory tests suggest that most sites within the Ninmaroo Formation are dolomitic. This observation is consistent with the diagenetic history of the Ninmaroo Formation presented by Radke (1982), wherein a protracted period of dolomitization, commencing in the Late Ordovician and associated with telogenesis (uplift and erosion), is described.

3 SAMPLING DETAILS AND LABORATORY METHODS

One hundred eighty-six palaeomagnetic sites were sampled in the Middle–Late Cambrian aged Chatsworth, Pomegranate and Devoncourt Limestones and the Cambrian–Ordovician Ninmaroo Formation. As palaeomagnetic sites are temporal, and not necessarily defined by spatial distribution, each sampled bed is treated as a single palaeomagnetic site. Of these, 87 beds were sampled at Mt Unbunmaroo (lateral distance across strike of 1300 m, sites GB10–GB19), 58 at Mt Datson (450 m sampled across strike, GB09), and 41 sites (GB01–GB08) in members of the Cambrian Chatsworth, Pomegranate and Devoncourt Limestones around the Chatsworth Station. All samples (two to three per bed) were obtained using a portable palaeomagnetic drill. Sampling was dictated primarily by exposure, with the distance between sampled sites ranging from 2 m to 35 m, and an average of 7 m between each site.

In the laboratory, cores were sliced into one to four specimens, 2.2 cm in height. Prior to demagnetization procedures, bulk susceptibilities were measured for all specimens. For all specimens the intensities and directions of the natural remanent magnetization (NRM) were determined using a horizontally mounted 2G755R DC SQUID magnetometer in the Rock Magnetism Laboratory at the Commonwealth Scientific and Industrial Research Organisation (CSIRO) in Sydney. Following the initial NRM measurement, at least two specimens per bed were treated with standard step-wise thermal and/or alternating field (AF) demagnetization, up to maximum temperatures and fields of 680 °C and 140 mT, respectively. Pilot AF and thermal demagnetization runs indicated that goethite, a magnetically 'hard' remanence carrier resistive to AF techniques, was a significant contributor to the remanence matrix for all samples. As such,

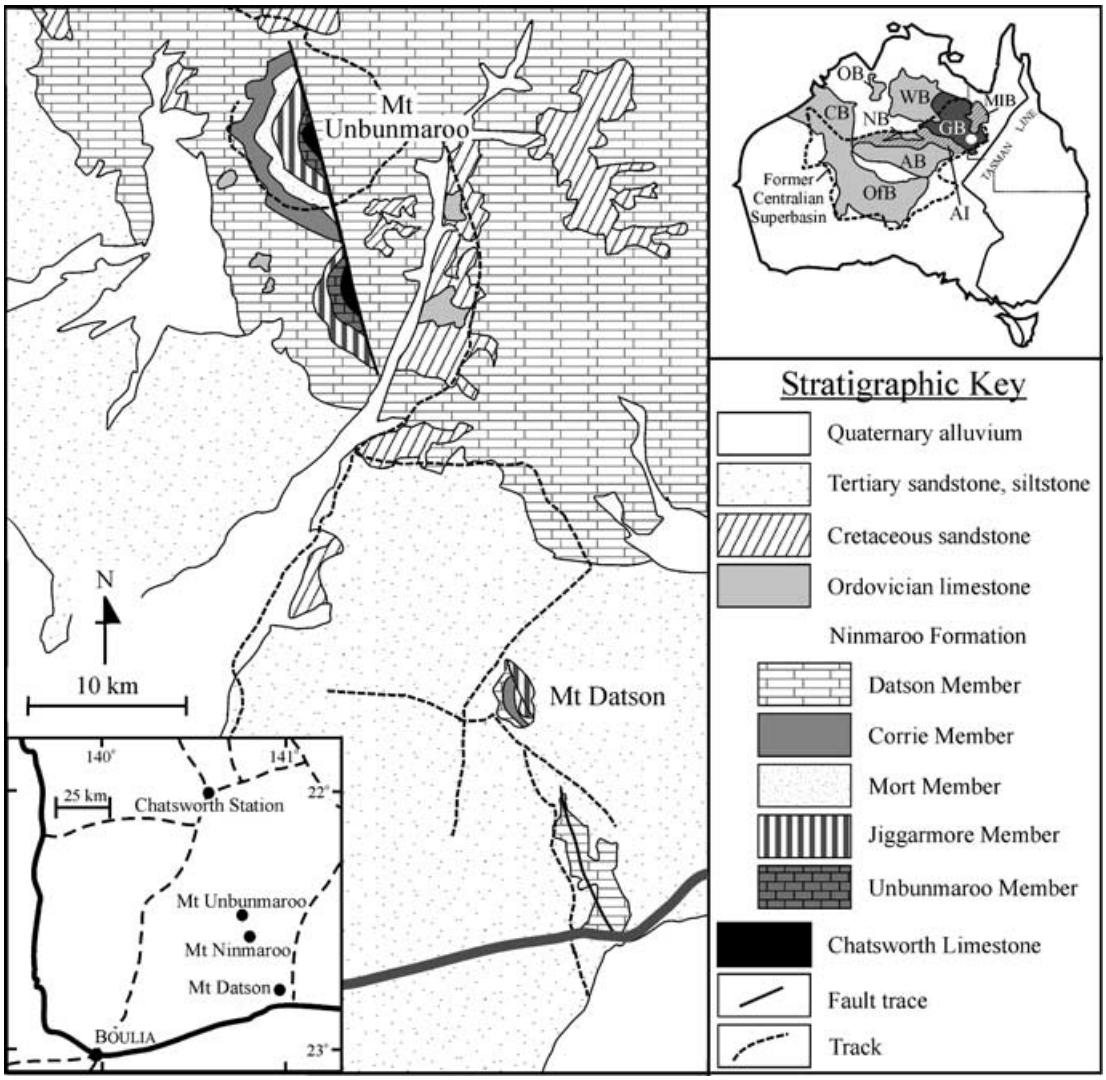

Figure 1. Simplified geology around Mts Unbunmaroo and Datson. Lower left inset shows relative location of Mts Unbunmaroo and Datson to Chatsworth Station. Upper right inset depicts the boundaries and structural elements of the Neoproterozoic-Early Palaeozoic Centralian Superbasin and their relation to the Palaeozoic Tasman Line. Sub-basin mnemonics are as follows: GB = Georgina Basin, WB = Wiso Basin, NB = Ngalia Basin, OB = Ord Basin, CB = Canning Basin, OfB = Officer Basin, AB = Amadeus Basin. AI and MIB designate the Proterozoic Arunta Inlier and Mt Isa Block, respectively. White circle in upper box denotes relative sample region.

prior to AF demagnetization all specimens were treated with a batch heating of 150 °C, the unblocking temperature for goethite being 120 °C (Dunlop & Özdemir 1997). Thermal steps were separated by 25 °C for temperatures less than 450 °C, after which heating increments were reduced to 20–10 °C, depending upon demagnetization behaviour. During AF demagnetization, applied fields were separated by 2 mT up to 20 mT after which demagnetization progressed by 5 mT steps until the signal had been completely randomized or maximum fields of 140 mT were reached.

Strong contributions from diamagnetic material, in particular calcite, precluded low-field anisotropy of magnetic susceptibility (AMS) studies on these limestones as bulk susceptibilities were highly variable, and generally not reproducible, and AMS results were inconsistent for multiple measurements on single samples.

In an attempt to better define remanence mineralogies, 88 specimens were dissolved in acetic acid for times ranging between 48 and 216 h to extract the magnetic minerals. (Acetic acid will dissolve calcite matrix in limestones, but will not affect any magnetite present, unlike hydrochloric acid.) Whilst dissolution provided detritus from most specimens, 32 were not appreciably affected, suggesting that these specimens were taken from highly dolomitized beds. Sediment from the remaining 56 specimens did not contain sufficient magnetic material for detailed rock magnetic investigations by means of the variable field translation balance housed at CSIRO. As such, assessments of remanence mineralogy were necessarily restricted to analyses of 3-D isothermal remanent magnetization (IRM) (Lowrie 1990) and palaeomagnetic results. Seventy-two specimens, 24 from each of the three sampling areas, were subjected to 3-D IRM, described below.

Demagnetization behaviour was monitored throughout via orthogonal vector diagrams (Zijderveld 1967) and equal-area stereographic projections. Principal component analysis (Kirschvink 1980) was used to determine characteristic and secondary magnetization components. Specimens for which components had maximum angular deviation (MAD) > 15°, or those displaying chaotic behaviour, were not included in later analyses. When linear segments

of demagnetization vectors could be identified (three points being the minimum used to define a linear segment), site-mean directions were calculated according to standard methods (Fisher 1953). Fold tests (McFadden 1998) and reversal tests (McFadden & Lowes 1981) were applied to resultant palaeomagnetic data from the three sampling regions in an effort to constrain magnetization ages. In addition, results from an applied clustering algorithm (McFadden 1998) are presented.

4 RESULTS

4.1 Rock magnetic results

For the step-wise thermal demagnetization of 3-D IRM (Lowrie 1990), the following fields were applied to each specimen: 1 T along the *z*-axis, 0.1 T along the *y*-axis and 0.01 T along the *x*-axis. Results from these tests reveal three characteristic demagnetization spectra (Fig. 2). The first is a nearly simultaneous decay of all three imparted components with specimens completely demagnetized by 550 °C (Figs 2a–c). This behaviour is associated with dolomitized samples, in particular those from beds in the Ninmaroo Formation, and was found only in samples coming from Mt Unbunmaroo and Mt Datson. Within the second subset (with unblocking temperatures (T_{ub}) $\approx$ 580 °C and median destructive fields (MDFs) of $\leq$60 mT), AF demagnetization and block-shouldered 3-D IRM demagnetization spectra for the fine-grained light-grey and dark-grey limestones beds, taken from all three sample areas, identify end-member pseudo single-domain (PSD) magnetite as the remanence carrier (Figs 2d, e). Occasionally, haematite is also seen in samples belonging to these lithological subsets (Fig. 2f). The third 3-D IRM group is generally associated with the reddish grey marls, but is also found in a few isolated samples from the light-grey limestone beds. Demagnetization behaviour of these samples suggests that the high-coercivity spectra (haematite) are dominant, with high unblocking temperatures of 650–680 °C (Figs 2g–i).

4.2 Palaeomagnetic results and interpretations

Extremely weak magnetizations, particularly after the removal of the goethite contribution, left approximately 25 per cent of all specimens too weak for continued AF or thermal demagnetization procedures. Indeed, sometimes up to 98 per cent of the initial NRM intensity for all specimens was held by goethite. NRM intensities could be as high as 3 mA m^{-1} while after the 150 °C step, values were more generally of the order of 0.1–0.04 mA m^{-1}. Characteristically weak magnetizations made stable directions difficult to identify and, as a general rule, AF demagnetization proved more effective in isolating magnetization components. Intensities for many of the thermally treated specimens fell below magnetometer sensitivity by 400 °C with components becoming too unstable to allow for further analysis.

In total, five characteristic remanence magnetizations (ChRMs) were revealed during this investigation. These included a normal polarity component (PF) defined by north with moderate up inclination directions and low to moderate unblocking temperatures and coercivities, which was generally removed by the 150 °C step. A second component (TR) is directed to the south(north) and down(up) with moderate to steep inclinations and was identified in 40 sites (55 samples). This component has high unblocking temperatures and coercivities. A northwest(southeast) and up(down) with shallow to very shallow inclination directions characterize component A. Component A has moderate unblocking temperatures and coercivities. Shallow to moderate inclinations and west–east directions typify the B component. Component B is the dominant magnetization component found within the Chatsworth and Ninmaroo Formations. Component C is directed to the northeast–southwest with moderate to shallow inclinations. This component has moderate to high unblocking temperatures and coercivities and was more readily identified using AF techniques than by thermal demagnetization.

Each of these components is discussed in detail below with representative orthogonal vector diagrams shown in Fig. 3. In the original study carried out at Mt Unbunmaroo (Ripperdan & Kirschvink 1992), four magnetization components were discussed. The discrepancy between that study and these findings is examined in the discussion following presentation of results and interpretations.

Components PF and TR

A chemical remanent magnetization is present in most sites, directed to the north with moderate inclination directions and is exclusively of normal polarity. This component (PF) tended to be removed by 150 °C, but could persist up to 300 °C with thermal demagnetization procedures. As this remanence was impervious to AF demagnetization but was generally unblocked by 150 °C, the PF component is thought to be held primarily by goethite. At the 95 per cent confidence interval this direction is indistinguishable from the present field direction expected in the sampling region and has a mean *in situ* direction of $D = 5.1°$, $I = -52.8°$, $n = 202$, $k = 27.9$, $\alpha_{95} = 1.9°$ (Fig. 4a, Table 1).

The dual-polarity TR component, identified in 40 sites (55 samples), is directed to the south(north) and down(up) with moderate to steep inclinations and unblocking temperatures in the haematite range ($T_{ub} \approx 680$ °C). Fig. 2(g) shows the characteristic 3-D IRM demagnetization spectra associated this ChRM. The reversal test (McFadden & Lowes 1981) is positive for TR, with a B classification (observed angle (γ_o) = 5.72°, critical angle (γ_c) = 11.29°). At the 95 per cent confidence interval, TR fails the fold test of McFadden (1998). The mean *in situ* direction of TR is $D = 10.4°$, $I = -54.1°$, $k = 20.9$, $\alpha_{95} = 4.3°$ (Fig. 4b, Table 1). This component was distinguished from the PF direction by its extreme stability, high unblocking temperatures, and simple linear decay to the origin on orthogonal projection diagrams; no other components were present in TR samples (Fig. 3a). The corresponding palaeopole, calculated from 40 VGPs, lies at $\lambda = 74.0°$S, $\phi = 107.7°$E, $dp = 4.2°$, $dm = 6.0°$, is consistent with the Tertiary segment of Australia's APWP and is most probably a reflection of widespread Tertiary weathering (Dunlop & Özdemir 1997) (magnetite commonly oxidizes to haematite in weathering environments). As components PF and TR are relatively recent acquisitions to the magnetic history of the Cambrian–Ordovician units within the eastern Georgina Basin, and have no bearing on Australia's Palaeozoic APWP, analysis of these magnetizations is not included in the ensuing discussion.

Component A

3-D IRM results for component A indicate that magnetite is the remanence carrier for this ChRM (Figs 2d and f). Component A is often found with PF, discussed above (Fig. 3b). In a few cases, component A gives way to component C magnetizations, discussed below, at high temperatures and fields (Fig. 3h). Figs 2(e) and (i) are characteristic 3-D IRM results from specimens containing both A and C components.

The dual-polarity A component has northwest/southeast directions and shallow inclinations and is found in one or two, and more rarely three, samples from 46 sites ($n = 70$) (Figs 3b , 3h). Mean

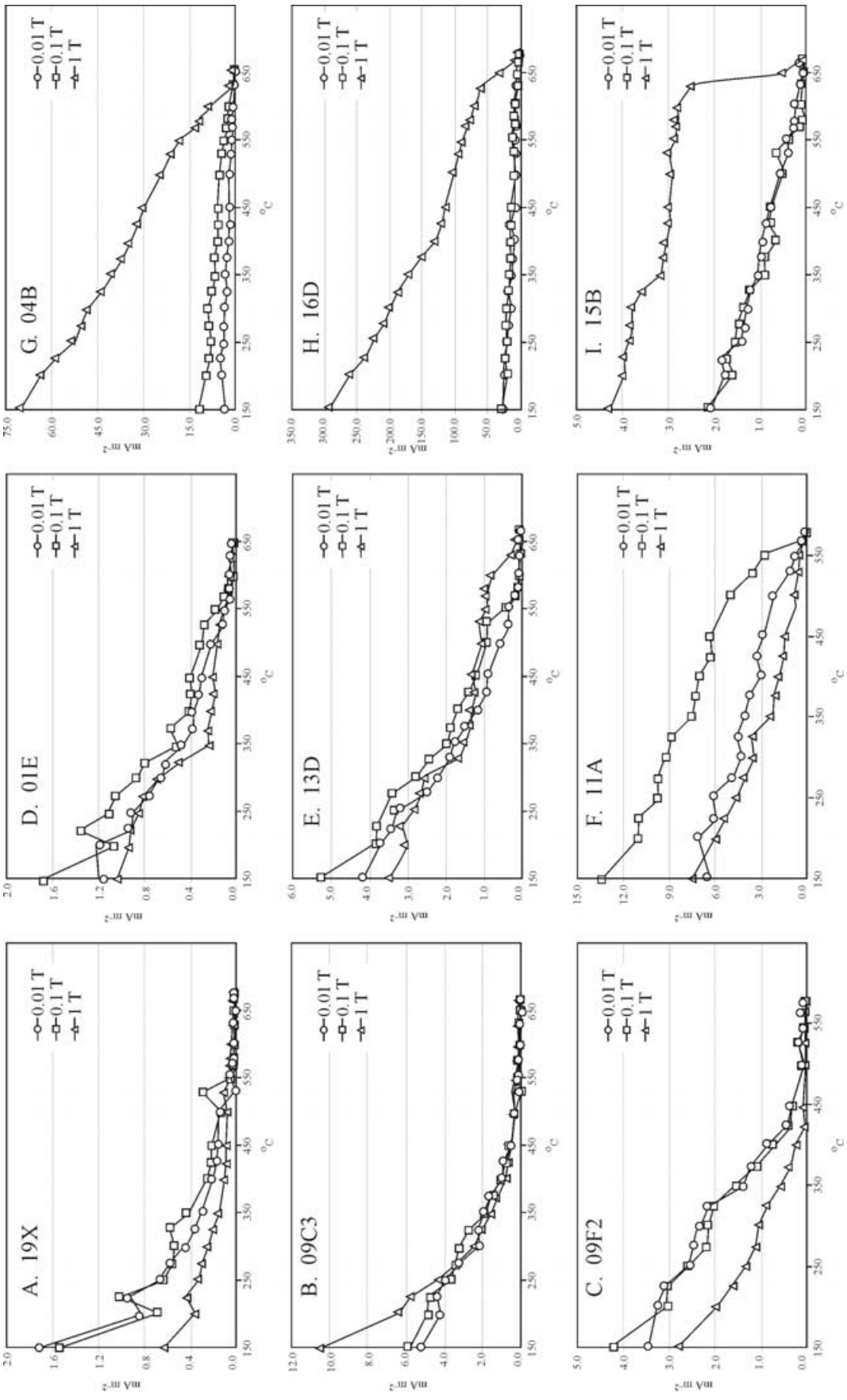

Figure 2. 3D-IRM results from the Chatsworth Limestone and Ninmaroo Formation. (a)–(c) spectra do not reveal a dominant remanence mineralogy. In examples (d)–(f), magnetite is dominant, although (d) and (e) suggest the presence of magnetic mineralogies with unblocking temperatures greater than 580∘C. In (g)–(i), haematite can be seen to govern the unblocking spectra.

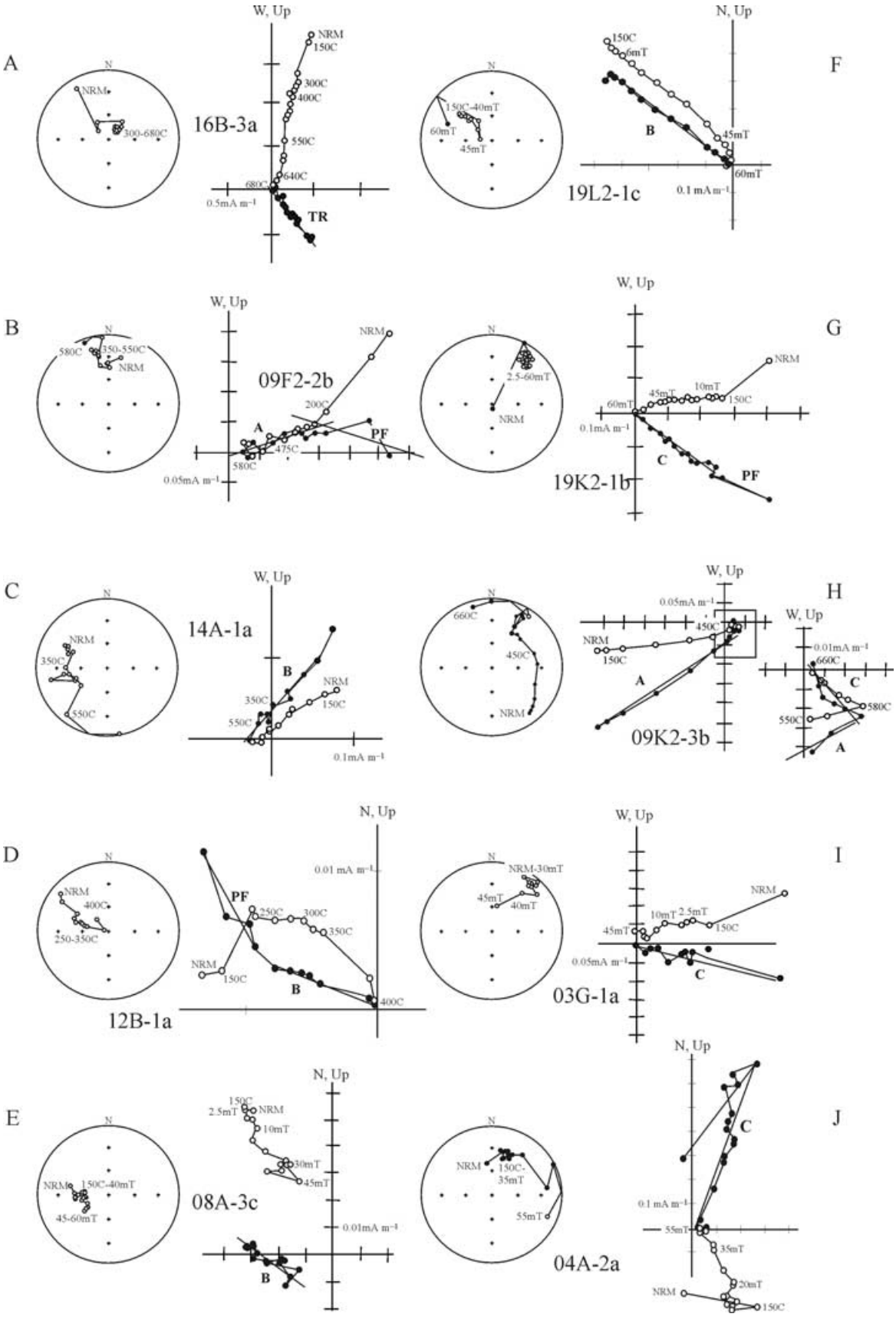

Figure 3. Demagnetization data from the Chatsworth Limestone and Ninmaroo Formation. Stereonets are equal-area projections in which open/closed circles represent upper/lower hemisphere projections. PF (present field), TR, A, B and C components, as discussed in the text, are labelled on each vector plot and directions are cited for each sample. (a) is shown in *in situ* coordinates, the remaining data are tilt-adjusted.

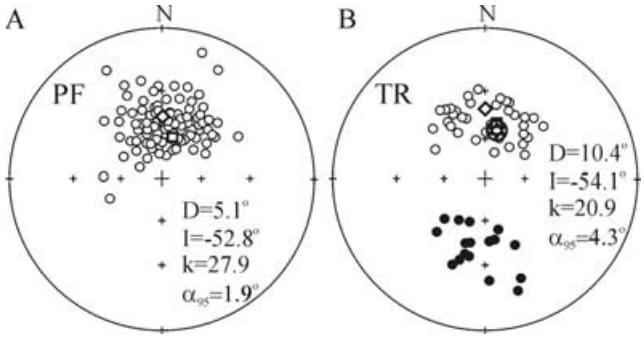

Figure 4. Mean directional data for PF (a) and TR (b) components. White diamonds and squares represent locations of the best-fitting dipole field (DF) and the present geomagnetic field (PF), respectively, in the sampling region. Star in (b) shows the mean location of the TR component with its associated uncertainty.

site-level data are presented in Table 2. Unblocking temperatures for this component range between 300 °C and 580 °C with MDFs of ∼40 mT. At the 95 per cent confidence interval these data have a positive fold test (McFadden 1998) with before and after tilt correction directions of $D = 330.8°$, $I = -0.9°$($k = 13.9$, $\alpha_{95} = 6.0°$) and $D = 330.6°$, $I = -3.9°$($k = 15.0$, $\alpha_{95} = 4.5°$) respectively (Figs 5a and b). Before tilt correction, normal and reverse data sets comprising the A ChRM have a B-class reversal test (McFadden & Lowes 1981) ($\gamma_o = 5.7°$, $\gamma_c = 9.1°$), while at 100 per cent unfolded, these data have an A classification ($\gamma_o = 2.73°$, $\gamma_c = 11.26°$). Using the tilt-adjusted data, the mean palaeomagnetic pole for component A lies at $\lambda = 54.7°$S, $\phi = 262.3°$E, ($dp = 2.3°$, $dm = 4.5°$) (Table 3).

4.2.1 Component B

West–east directions with moderate to shallow inclinations characterize the B component. B is the most widespread magnetization within the sample area, found in 77 sites (115 samples). Component B directions are more readily identified in thermally demagnetized specimens and generally become randomized at temperatures less than 400 °C and destructive fields of ≤20 mT. The mean *in situ* and tilt-adjusted directions for component B are: $D = 271.4°$, $I = -14.7°$($k = 5.6$, $\alpha_{95} = 7.4°$); $D = 272.4°$, $I = -27.6°$($k = 9.9$, $\alpha_{95} = 5.3°$), respectively (Figs 5C and 5d, Table 3).

In situ data pass the reversal test of McFadden & Lowes (1981) with a C classification, $\gamma_o = 13.0°$, $\gamma_c = 17.8°$. At 100 per cent unfolded, however, component B normal and reverse data have a negative reversal test, $\gamma_o = 13.3°$, $\gamma_c = 11.2°$. Fold test statistics (McFadden 1998) for the B component are ambiguous, suggesting that the magnetization could have been acquired *in situ*or at 100 per cent tilt-adjusted. It is thought that the reason for this is the near coincidence of the *in situ* and tilted declinations with the strike of folding, making this direction insensitive to the applied test. Incongruent precisions for component B in each of the sampled limbs also prohibit a meaningful application of the fold test (McFadden 1998; McFadden & Jones 1981). Uncertainty surrounding the results from these two tests could be the result of unrecognized structural complications within this area and/or the failure to completely remove competing magnetization spectra.

The *in situ* data yield a palaeopole at $\lambda = 4.1°$S, $\phi = 224.3°$, $dp = 3.9°$, $dm = 7.6°$. Using tilt-adjusted data, the resultant palaeopole lies at $\lambda = 8.0°$S, $\phi = 216.8$E° ($dp = 2.6°$, $dm = 5.1°$) (Table 3). These two poles are separated by 14.2° and while both fall upon the Late Ordovician–Early Silurian segment of the APWP they are dissimilar at the 95 per cent confidence interval. Although results from the applied fold test were inconclusive, and have marginal results from applied reversal tests, visual inspection of site-mean data (Figs 5c and d) and comparison of before and after tilt adjustment precision values ($k_{insitu} = 5.6$, $k_{\text{tilted}} = 9.9$) indicate that the data are slightly better grouped at 100 per cent untilting. As such, the palaeopole associated with the tilted data (sgb in Fig. 8) has been preferentially chosen to reflect this remanence direction.

In general, samples characterized by the B ChRM had the weakest magnetization intensities, NRM intensities ≈ 0.01 mA m^{-1}, as opposed to values around 0.5 mA m^{-1} found in samples described by other ChRMs. There were, however, a few sites (about 5 per cent of those used in palaeomagnetic analyses) that had anomalously strong intensities (NRM intensities ≥0.3 mA m^{-1}). Specimens from these sites were also typified by extremely stable univectorial decay trajectories (Fig. 3f). More typically, the B direction is found with the PF direction, and in these cases B ChRMs tend to move away from, or fail to reach, the origin (Figs 3c–e), suggesting that this component is most probably not primary in origin. 3-D IRM spectra for component B-related samples (Figs 2a–c) show that this component is completely demagnetized by 550 °C. As the intensities of these

Table 1. Mean directional data for the PF and TR components. Explanation of table headings: mean directions are listed for each of the three sampling areas, as well as combined mean directions. Latitude (°S)/Longitude (°E) give the mean location of each sampling area; *n* represents the number of samples used in palaeomagnetic analysis; *D* (°) and *I* (°) give the *in situ* declination and inclination of the respective components; *k* and α_{95} are standard Fisherian parameters (Fisher 1953); λ (°N) and ϕ (°E) give the location of the palaeomagnetic pole calculated from mean directional data; *dp*(°)/*dm*(°) correspond to the semiaxes of uncertainty associated with each calculated palaeomagnetic pole at the 95 per cent confidence interval.

Components for each of the three sampled areas	Latitude (°S)	Longitude (°E)	*n*	*In situ* directions D (°)	I (°)	*k*	α_{95} (°)	λ (°N)	ϕ (°E)	*dp* (°)	*dm* (°)
PF											
Black Mountain	22.6	140.3	56	9.4	−53.5	14.7	7.6				
Mt Datson	22.8	140.4	112	1.5	−52.5	42.4	3.1				
Chatsworth Station	21.9	140.1	33	10.8	−52.2	44.3	6				
Mean direction			202	5.1	−52.8	27.9	1.9				
Mean pole *in situ*								−78.0	119.3	2.7	3.9
TR											
Black Mountain	22.6	140.3	24	2.2	−57.5	16.8	7.4				
Mt Datson	22.8	140.4	5	335.2	−48.1	179.5	5.7				
Chatsworth Station	21.9	140.1	26	13.7	−56.3	27.1	5.5				
Mean direction			55	2.8	−57.2	11.5	7.1				
Mean pole *in situ*								−74.3	131.9	7.5	10.3

Table 2. Site mean data for components A, B and C. Palaeomagnetic components from the eastern Georgina Basin. Explanation of table headings: Site: palaeomagnetic site; FM is the sampled formation (from oldest to youngest these are: ЄMD = Devoncourt Lmst; ЄMR = Pomegranate Lmst; ЄUC = Chatsworth Lmst; ЄUCL = Lily Creek Member, Chatsworth Lmst; ЄONU = Unbunmaroo Member, Ninmaroo Fm; ЄONJ = Jiggamore Member, Ninmaroo Fm); Latitude (°S)/Longitude (°E) denote latitude/longitude positions for palaeomagnetic sites; *n* is the total number of samples used in analysis for each site; *in situ* Dec. (°)/Inc. (°) are the *in situ* declination and inclination in degrees; Strike and Dip are structural corrections; 100 per cent unfolded Dec. (°)/Inc. (°) are the tilt-corrected declination and inclination directions; α_{95} is the half-angle of the 95 per cent confidence cone, calculated for sites with $n \geq 3$. Mean data, *in situ* and tilt-corrected, are presented for each of the three sampling regions and also as overall mean results. In these summary tables, Latitude (°S)/Longitude (°E) give regional mean geographic location; *N*/*n* refers to the number of site/samples used in analyses; *in situ* and 100 per cent unfolded values are given for *D* (°)/*I* (°) (mean declination/inclination); *k* and α_{95} (standard Fisherian statistics) (Fisher 1953). Component mean directions are also included in Table 3 in a more readily accessible format.

Component A					*In situ*				100 per cent unfolded		
Site	FM	Latitude (°S)	Longitude (°E)	*n*	Dec. (°)	Inc. (°)	Strike	Dip	Dec. (°)	Inc. (°)	α_{95} (°)
10	ЄUC	22.6	140.3	3	152.2	−31.9	0	0	152.2	−31.9	4.8
11A	ЄUC	22.6	140.3	3	336.6	1.5	171.6	10	336.6	−1.1	6.6
11D	ЄUC	22.6	140.3	1	335.3	12	141.6	8	336.8	−10	––
13A	ЄUC	22.6	140.3	1	327.2	−5.7	156.6	6	327.8	−6.6	—
13D	ЄUC	22.6	140.3	1	145.5	−23.3	166.6	12	150.9	27.1	—
15C	ЄUC	22.6	140.3	2	339	1.2	157.6	7	339.1	−1	—
15B	ЄUC	22.6	140.3	1	334.4	−1.5	157.6	7	334.6	−1.9	—
16E	ЄUC	22.6	140.3	1	313.6	−0.4	156.6	5	313.7	−2.4	—
16C	ЄUC	22.6	140.3	1	350.1	−7.3	156.6	5	350.7	−6.1	—
17	ЄUC	22.6	140.3	3	337.4	20.4	151.6	4	338.9	−19.9	18.7
18F	ЄUCL	22.6	140.3	1	124.4	−12.9	156.6	8	126.2	17.1	—
18E	ЄUCL	22.6	140.3	1	353.7	4	156.6	8	353	6.3	—
18D	ЄUCL	22.6	140.3	2	154.7	−4.7	156.6	8	154.1	−4.4	—
19C	ЄONJ	22.5	140.3	1	323.7	−9.1	130.6	8	322.3	10.8	—
19E	ЄONJ	22.5	140.3	1	133.3	−19.6	130.6	8	136.1	19	—
19H	ЄONJ	22.5	140.3	1	151.9	−14.3	130.6	8	153.6	11.3	—
19I	ЄONJ	22.5	140.3	1	159.2	4.7	130.6	8	159.5	0.8	—
19M	ЄONJ	22.5	140.3	2	146.7	2.5	39.6	12	146.9	−9	—
19Q	ЄONJ	22.5	140.3	2	139	−2.6	238.6	5	139	2.3	—
19W	ЄOCU	22.5	140.3	1	299.5	2.5	307.6	4	299.3	−1.9	—
19H2	ЄOCU	22.6	140.3	1	148.5	24.1	111.6	8	151	19.2	—
01H	ЄUC	22.0	140.3	2	159.5	−20.1	96.6	4	160.1	16.5	—
01E	ЄUC	22.0	140.3	1	328	−2.7	74.6	5	328	2.1	—
02D	ЄUC	22.0	140.3	1	349	6.7	84.6	5	349	−1.7	—
02C	ЄUC	22.0	140.3	1	142.1	−3	84.6	5	141.9	−7.2	—
03N	ЄUC	22.0	140.3	1	326.8	20.1	0	0	326.8	20.1	—
03K	ЄUC	22.0	140.3	1	344.3	20	0	0	344.3	−20	—
03I	ЄUC	22.0	140.3	1	345.8	5	0	0	345.8	5	—
03H	ЄUC	22.0	140.3	1	166.2	−6.6	0	0	166.2	6.6	—
03E	ЄUC	22.0	140.3	4	337.7	3.4	0	0	337.7	−3.4	12.6
03D	ЄUC	22.0	140.3	2	135.7	−27.6	246.6	5	134.6	32.3	—
04D	ЄMD	21.3	140.1	1	304.7	10.1	66.5	4	305	−6.7	—
09C3	ЄUC	22.8	140.4	2	318.6	−8.9	171.7	45	333.5	−29.4	—
09K2	ЄUC	22.8	140.4	2	140.1	20.5	174.7	45	165.2	38.6	—
09U2	ЄUC	22.8	140.4	2	146.1	−43	174.7	45	126	−13.6	—
09D3	ЄUC	22.8	140.4	1	333.3	−11.1	161.7	45	343.8	−13.7	—
09F2	ЄUC	22.8	140.4	1	309.5	22.9	169.7	39	304.6	−4.1	—
09G2	ЄUC	22.8	140.4	3	164.4	15	169.7	39	175.3	14.9	—
09H2	ЄUC	22.8	140.4	3	167.2	−15	169.7	39	158.2	−10.1	3.6
09K2	ЄUC	22.8	140.4	1	145.2	−18	174.7	45	141.1	6.5	—
09B3	ЄUC	22.8	140.4	1	306.3	14.6	147.7	33	302	1.1	19.1
09B	ЄONU	22.8	140.4	1	353.8	21.4	154.5	30	340	28	—
09C	ЄONU	22.8	140.4	2	166.1	6.5	154.5	30	167.8	−0.1	—
09E	ЄONU	22.8	140.4	1	182	−18.6	154.5	30	169.1	−29.7	—
09M	ЄONU	22.8	140.4	1	313.7	33	178.7	50	305.3	−6	—
09O	ЄONU	22.8	140.4	2	333.6	22.1	178.7	50	325.9	−3.4	—

Mean data	Latitude	Longitude		*In situ*				100 per cent unfolded			
Component A	(°S)	(°E)	*N*/*n*	*D* (°)	*I* (°)	*k*	α_{95}(°)	*D* (°)	*I* (°)	*k*	α_{95}(°)
BM	22.6	140.3	21/31	328.9	−4.9	20.5	7.4	329.9	−4.2	11.9	9.9
MD	22.8	140.4	14/23	332.2	10.4	10.1	14.4	330.0	−2.2	9.7	14.6
CS	21.9	140.1	11/16	332.9	−6.5	11.0	19.6	330.0	−4.9	17.8	11.7
Mean direction			46/70	330.8	−0.9	13.9	6.0	330.6	−3.9	15.0	5.8

Table 2. (*Continued*).

Component A					*In situ*				100 per cent unfolded		
Site	FM	Latitude (°S)	Longitude (°E)	*n*	Dec. (°)	Inc. (°)	Strike	Dip	Dec. (°)	Inc. (°)	α_{95} (°)
09C	ЄONU	22.8	140.4	1	283.3	−5.3	154.5	30	289.4	−27.9	—
09H	ЄONU	22.8	140.4	1	249	15.5	187.7	33	249.3	−13.7	—
09I	ЄONU	22.8	140.4	1	75	15.3	187.7	33	66	44.9	—
09O	ЄONU	22.8	140.4	1	302.5	41.2	178.7	50	293.5	−3.2	—
09P	ЄONU	22.8	140.4	1	79.2	−8.8	178.7	50	76.3	40.4	—
09Q	ЄONU	22.8	140.4	2	69.9	−18.2	178.6	50	68.2	29.2	—
09W	ЄONU	22.8	140.4	1	98.7	5.3	176.6	47	105.9	50.8	—
09Y	ЄONU	22.8	140.4	3	254.9	40.5	176.6	47	257.7	−5.8	9.5
09Z	ЄONJ	22.8	140.4	1	268.7	44.1	176.6	47	268.1	−2.9	—
09A2	ЄONJ	22.8	140.4	2	300.4	30.6	169.7	39	293.8	−0.9	—
09B2	ЄONJ	22.8	140.4	2	269.8	22.2	169.7	39	269.4	−16.3	—
09C2	ЄONJ	22.8	140.4	1	300.3	26.6	169.7	39	295.4	−4.5	—
09F2	ЄONJ	22.8	140.4	2	110.1	−32.9	169.7	39	104.9	1.9	—
09G2	ЄONJ	22.8	140.4	1	70.4	−10.8	169.7	39	69.4	27.7	—
09M2	ЄUC	22.8	140.4	1	298	2.3	174.7	45	306.3	−34.2	—
09O2	ЄUC	22.8	140.4	2	285.3	27	174.7	45	283.7	−15.6	—
09P2	ЄUC	22.8	140.4	3	96.8	−36.9	174.7	45	94.4	7.4	3.9
09Q2	ЄUC	22.8	140.4	2	73.8	−16.4	174.7	45	72.9	27.8	—
09R2	ЄUC	22.8	140.4	1	69.7	−56.6	174.7	45	76.3	−12.4	—
09S2	ЄUC	22.8	140.4	2	287.6	5.8	174.7	45	293	−35.2	—
09B3	ЄUC	22.8	140.4	2	296.7	16.4	147.7	33	293.1	−1.9	—
09C3	ЄUC	22.8	140.4	1	300.1	2.4	171.7	45	308.5	−31.6	—
09D3	ЄUC	22.8	140.4	1	268.3	52.4	161.7	45	261.8	8.4	—
19C	ЄONJ	22.5	140.3	1	68.4	−4.6	130.6	8	68.3	2.5	—
19D	ЄONJ	22.5	140.3	1	268.8	−51.4	130.6	8	277.5	−56.3	—
19E	ЄONJ	22.5	140.3	1	276.7	−11.8	130.6	8	278.4	−16.2	—
19H	ЄONJ	22.5	140.3	1	268.1	−15.2	130.6	8	207	−20.5	—
19I	ЄONJ	22.5	140.3	1	274	−4.5	130.6	8	274.8	−9.2	—
19O	ЄONJ	22.5	140.3	2	75.4	36.9	238.6	5	71.7	38.2	—
19Q	ЄONJ	22.5	140.3	2	96.2	18.3	238.6	5	94.8	21.3	—
19T	ЄONJ	22.5	140.3	1	111.2	12.4	239.6	8	109.8	18.6	—
19W	ЄONU	22.5	140.3	1	262.6	−0.3	307.6	5	262.7	3.2	—
19X	ЄONU	22.5	140.3	1	56.6	15.4	307.6	4	56.3	11.6	—
19Y	ЄONU	22.5	140.3	1	51.8	16.1	176.6	6	50.6	21	—
19B2	ЄONU	22.5	140.3	1	86.3	10	54.6	6	87.1	6.8	—
19H2	ЄONU	22.6	140.3	1	243.1	−28.3	111.6	8	246.4	−34.1	—
19J2	ЄONU	22.6	140.3	1	313.7	−37.8	111.6	8	319	−34.4	—
19L2	ЄONU	22.6	140.3	1	306.1	−31.9	111.6	8	310.7	−29.6	—
19N2	ЄONU	22.6	140.3	1	95.6	7.6	121.6	4	96.1	9.3	—
18H	ЄUCL	22.6	140.3	1	265.8	−12.1	158.6	5	266.2	−16.9	—
18E	ЄUCL	22.6	140.3	1	225	−29.4	156.6	8	223	−36.8	—
18D	ЄUCL	22.6	140.3	1	303.3	−28.3	156.6	10	308.5	−33.4	—
18A	ЄUCL	22.6	140.3	1	268.2	−44.6	166.6	16	273.3	−60.1	—
17	ЄUC	22.6	140.3	5	86.4	29.5	151.6	4	87.4	33.1	6.9
16D	ЄUC	22.6	140.3	3	104	24.8	156.6	5	105.6	28.7	15.1
14B	ЄUC	22.6	140.3	1	312.8	−44.5	132.6	8	320.6	−43.9	—
14A	ЄUC	22.6	140.3	2	266.4	−33.6	143.6	4	268	−36.9	—
13F	ЄUC	22.6	140.3	1	266.1	−29.2	166.6	12	267.6	−41	—
13A	ЄUC	22.6	140.3	3	271.4	−7.3	156.6	6	271.8	−12.7	10.8
12E	ЄUC	22.5	140.3	2	256.8	−25.3	163.6	10	257.1	−35.3	—
12D	ЄUC	22.5	140.3	1	91.1	11	163.6	10	92	20.5	—
12B	ЄUC	22.5	140.3	1	285.8	−20.1	165.6	13	289.1	−31.2	—
11C	ЄUC	22.6	140.3	1	266.2	−24.4	165.6	7	266.9	−31.3	—
11B	ЄUC	22.6	140.3	1	234.6	−27.4	165.6	7	233.1	−33.9	—
10	ЄUC	22.6	140.3	4	97.1	30.4	0	0	97.1	30.4	6.8

specimens tend to fall below magnetometer sensitivity by 400 °C or 20 mT, it is unclear whether the isolation of this direction, with respect to other components, is the result of fully demagnetizing a single dominant remanence carrier or if, instead, it merely reflects intensities that fell below magnetometer sensitivity, hindering resolution of a third component.

Component C

Twenty-seven sites within the Cambrian Chatsworth ($N = 23$) and Devoncourt Limestones ($N = 4$) and 14 sites within the lower members of the Cambrian–Ordovician Ninmaroo Formation have component C as the ChRM direction ($N = 42$, $n = 96$). This component

Table 2. (*Continued.*)

Component B					*In situ*				100 per cent unfolded		
Site	FM	Latitude (°S)	Longitude (°E)	*n*	Dec. (°)	Inc. (°)	Strike	Dip	Dec. (°)	Inc. (°)	α_{95} (°)
07A	€MR	23.8	140.0	2	265.7	−54.1	38.4	11.5	274.1	−45.1	—
07B	€MR	23.8	140.0	1	295.2	−45.9	21.2	9	294.7	−36.9	—
08D	€MD	21.4	140.0	1	279.5	−19.7	30.7	8	280.3	−12.2	—
08C	€MD	21.4	140.0	1	304.9	−51.9	51.6	6	306.8	−46.1	—
08B	€MD	21.4	140.0	1	250.6	9.9	47	5	249.7	11.9	—
08A	€MD	21.4	140.0	2	271	−58.3	43.9	7.5	277.9	−52.5	—
05C	€MD	21.3	140.1	1	53.5	39.6	21.4	9	59.1	34.4	—
05B	€MD	21.3	140.1	1	289.9	−28.9	21.4	9	290	−19.9	—
04C	€MD	21.3	140.1	2	269.5	−30.4	66.5	4	271.6	−28.8	—
04B	€MD	21.3	140.1	2	266.5	−30.4	76.5	2	267.6	−30	—
04A	€MD	21.3	140.1	1	319.4	−51	76.5	2	320.5	−49.2	—
03M	€UC	22.0	140.3	1	75.9	45.8	0	0	75.9	45.8	—
03L	€UC	22.0	140.3	1	250.3	−8.9	0	0	250.3	−8.9	—
03J	€UC	22.0	140.3	1	99.4	32.1	0	0	99.4	32.1	—
03I	€UC	22.0	140.3	2	266.8	−11.2	0	0	266.8	−11.2	—
03F	€UC	22.0	140.3	1	284.9	−42.8	0	0	284.9	−42.8	—
03D	€UC	22.0	140.3	1	298.3	−19.4	0	0	298.3	−19.4	—
03C	€UC	22.0	140.3	3	292.4	−31.3	246.6	5	290.1	−34.8	16
03A	€UC	22.0	140.3	3	241.9	−39.2	246.6	5	237.9	−38.6	14.7
01C	€UC	22.0	140.3	3	251.7	−39.8	101.5	3	254	−41.2	4.5
01B	€UC	22.0	140.3	1	72.3	34.7	101.5	3	74.2	36.1	—
01A	€UC	22.0	140.3	1	122.8	21.9	101.5	3	123.9	20.8	—

Mean data	Latitude	Longitude		*In situ*				100 per cent unfolded			
Component B	(°S)	(°E)	*N*/*n*	*D* (°)	*I* (°)	*k*	α_{95}(°)	*D* (°)	*I* (°)	*k*	α_{95}(°)
BM	22.6	140.3	32/47	267	−26.5	11.3	7.8	268.5	−31.7	10.4	8.1
MD	21.9	140.1	23/35	276	23.5	9.5	10.1	275.4	−17.1	10	9.8
CS	22.8	140.4	22/33	273	−35.2	11	9.8	274.6	−32.7	11.1	9.7
Mean direction			77/115	271	−14.7	5.6	7.4	272.4	−27.6	9.9	5.3

Mean data	Latitude	Longitude		*In situ*				100 per cent unfolded			
Component C	(°S)	(°E)	*N*/*n*	*D* (°)	*I* (°)	*k*	α_{95}(°)	*D* (°)	*I* (°)	*k*	α_{95}(°)
09L	€ONU	22.8	140.4	2	25.6	3.9	178.7	30	20.6	16.5	—
09O	€ONU	22.8	140.4	2	9.8	5.5	178.7	50	1.6	12	—
09S	€ONU	22.8	140.4	3	48.2	−31	178.7	60	52.9	17.9	3.9
09T	€ONU	22.8	140.4	2	215.7	3.5	178.7	60	202.6	−29.3	—
09U	€ONU	22.8	140.4	4	34.2	−19.7	178.7	60	35.1	17.8	6.3
09V	€ONU	22.8	140.4	4	30.8	−15.6	178.7	60	29.6	18	15.9
09W	€ONU	22.8	140.4	3	50.3	−5.4	176.7	47	42.9	31.5	8.2
09X	€ONU	22.8	140.4	2	195	26.7	176.7	47	208.2	5.8	—
09Y	€ONU	22.8	140.4	1	211.1	17	176.7	47	213.1	−11.3	—
09K2	€UC	22.8	140.4	1	31.8	−25.1	174.7	45	38.6	5.6	—
09N2	€UC	22.8	140.4	3	20.2	5.3	174.7	45	9.5	21.6	5.5
09T2	€UC	22.8	140.4	2	13.4	1.4	174.7	45	7.2	14.1	—
09V2	€UC	22.8	140.4	3	17.6	6	174.7	45	7	20.3	12.8
19C	€ONJ	22.5	140.3	2	20.8	14.9	130.6	8	19.9	22.4	—
19G	€ONJ	22.5	140.3	1	38.1	8.9	130.6	8	38	16.9	—
19H	€ONJ	22.5	140.3	2	39.1	30.2	130.6	8	39	38.2	—
19J	€ONJ	22.5	140.3	1	37.6	−0.7	130.6	8	37.6	7.3	—
19K2	€ONU	22.6	140.3	3	40.9	−5.8	111.6	8	40.8	−7.6	20.1
19P2	€ONU	22.6	140.3	3	22.1	17.9	121.6	4	21.9	21.8	8.9

is of dual polarity but is characterized by a reverse polarity northeast direction with shallow inclinations and a simple linear decay to the origin on orthogonal projection diagrams. The C ChRM is often found with PF, and occasionally with A, as discussed above (Figs 3g–j). Site-level data are presented in Table 2. The remanence carrier for the C component is predominantly magnetite ($T_{ub} \approx 580$ °C, MDF ≈ 35 mT), although this direction is also observed to persist in a few cases up to 680°C. Figs 2(d) and (i) show 3-D IRM spectra for sites containing the both C and A ChRMs, suggesting that magnetite and haematite contribute to these remanence directions. When the C component is found without the A ChRM, Fig. 2H shows a typical 3-D IRM response. Component C is most

Table 2. (*Continued*).

Component C, continued					*In situ*				100 per cent unfolded		
Site	FM	Latitude (°S)	Longitude (°E)	*n*	Dec. (°)	Inc. (°)	Strike	Dip	Dec. (°)	Inc. (°)	α_{95} (°)
16D	ЄUC	22.6	140.3	3	214.9	−11.1	156.6	5	214.3	−15.3	9.8
16C	ЄUC	22.6	140.3	1	48.7	−1.7	156.6	5	48.7	3.1	—
15B	ЄUC	22.6	140.3	3	26.8	11	157.6	7	25.7	16.3	15.6
15A	ЄUC	22.6	140.3	3	58.4	0.6	157.6	14	58.1	14.4	9.8
14C	ЄUC	22.6	140.3	2	219.7	3.3	111.6	11	219.8	−7.2	—
13D	ЄUC	22.6	140.3	2	206.7	2.5	166.6	12	206.5	−5.2	—
13B	ЄUC	22.6	140.3	2	45	0.3	172.6	13	44.2	10.6	—
12E	ЄUC	22.5	140.3	1	44.6	−8.2	163.6	10	44.9	0.6	—
12D	ЄUC	22.5	140.3	3	221.8	−3.2	163.6	10	221.1	−11.7	16
12A	ЄUC	22.5	140.3	2	211.7	−6.8	184.6	8	210.6	−10.4	—
08D	ЄMD	21.4	140.0	2	30.3	9.3	30.7	8	31.6	9.3	—
08D	ЄMD	21.4	140.0	2	190.5	−13.7	30.7	8	192.5	−16.3	—
05A	ЄMD	21.3	140.1	1	194.5	−28.4	21.4	9	199.4	−29.1	—
04A	ЄMD	21.3	140.1	3	14.8	30.4	76.5	2	15.4	32.2	11.9
03N	ЄUC	22.0	140.3	2	13.3	8.8	0	0	13.3	8.8	—
03J	ЄUC	22.0	140.3	1	33.3	2.2	0	0	33.3	2.2	—
03G	ЄUC	22.0	140.3	2	29.1	−1.4	0	0	29.1	−1.4	—
02C	ЄUC	22.0	140.3	3	11.6	8	84.6	5	11.9	12.8	7.3
01G	ЄUC	22.0	140.3	3	39.1	27.1	96.6	4	40.3	30.5	10.6
01E	ЄUC	22.0	140.3	4	208.7	−14.7	101.5	3	209	−17.6	15.4
01D	ЄUC	22.0	140.3	2	15.2	8.3	101.5	3	15.2	11.3	—
01C	ЄUC	22.0	140.3	2	27.6	15.2	101.5	3	27.9	18.1	—
01B	ЄUC	22.0	140.3	3	22.1	8.9	101.5	3	22.2	11.8	19.1

Component C

	Latitude	Longitude	*N*/*n*	*In situ*				100 per cent unfolded			
Mean data	(°S)	(°E)		*D* (°)	*I* (°)	*k*	α_{95}(°)	*D* (°)	*I* (°)	*k*	α_{95}(°)
BM	22.6	140.3	16/34	37.2	5.2	33.1	6.5	37	12.8	35.4	6.3
MD	22.8	140.4	13/32	27.4	−8.2	19.3	10.1	23.8	18.1	21.2	9.7
CS	21.9	140.1	13/30	22.3	13.5	36.5	7	23.1	15.5	35.6	7.9
Mean direction			42/96	29.7	4	19.7	5.2	28.8	15.3	35.7	4.5

Table 3. Mean Palaeozoic palaeomagnetic data for this study and that of Ripperdan & Kirschvink (1992) showing mean *in situ* and tilt-adjusted directions and resultant palaeomagnetic poles. Also shown are the difference between mean data from the two studies (subtended angle). Note that the polarities for the CO1° and the OVP[1] palaeopoles have been inverted to their antipode to make direct comparison more readily accessible. This has also been done for the tilt-corrected mean direction of the OVP[1] component of Ripperdan & Kirschvink (1992). Heading explanations are as in Table 2.

Component	*In situ* directions					Tilt-corrected directions							
	N	*D* (°)	*I* (°)	*k*	α_{95} (°)	*D* (°)	*I* (°)	*k*	α_{95} (°)	λ (°N)	ϕ (°E)	*dp* (°)	*dm* (°)
Component A	44	330.8	−0.9	13.9	6.0	330.6	−3.9	15.0	5.8	−54.9	261.6	2.9	5.8
OVP[2]	8	330.5	5.8	9.9	16.2	333.5	−17.7	10.7	11.4	−59.9	256.2	32.6	17.2
Subtended angle		6.7°				14.1°				7.8°			
Component B	78	271.4	−14.7	5.6	7.4	272.4	−27.6	9.9	5.3	−8.0	216.8	2.6	5.1
CO1°	64	271.8	24.2	5.8	8.1	274.5	4.3	6.7	7.4	−3.1	234.1	14.8	7.4
Subtended angle		38.9°				32.2°				17.9°			
Component C	41	29.7	4.2	19.7	5.2	28.8	15.4	35.7	4.5	48.6	186.0	2.1	4.0
OVP[1]	17	24.7	14.8	8.8	12.7	19.9	7.5	10.7	15.5	57.2	179.3	22.7	11.5
Subtended angle		11.9°				11.7°				9.5°			

often associated with the fine-grained dark-grey and reddish grey lithologies.

While directions and statistics do not change appreciably after unfolding, a positive fold test (McFadden 1998) for component C indicates a better grouping after unfolding. Mean *in situ* and tilt-adjusted directions are: $D = 29.7°$, $I = 4.0°$($k = 19.7$, $\alpha_{95} = 5.2°$); $D = 28.8°$, $I = 15.3°$($k = 35.7$, $\alpha_{95} = 4.5°$), respectively (Figs 5e and f, Table 2). Statistics for the reversal test (McFadden & Lowes 1981) are also positive for the C component, and like the fold test results, do not change appreciably after tectonic correction. *In situ* and tilt-adjusted statistics are $\gamma_o = 2.86°$, $\gamma_c = 11.79°$ and $\gamma_o = 2.23°$, $\gamma_c = 10.2°$, respectively, and are both rated as class A. The minor changes in statistics for both the reversal and fold tests are the consequence of bedding being subhorizontal or only shallowly dipping at 29 of

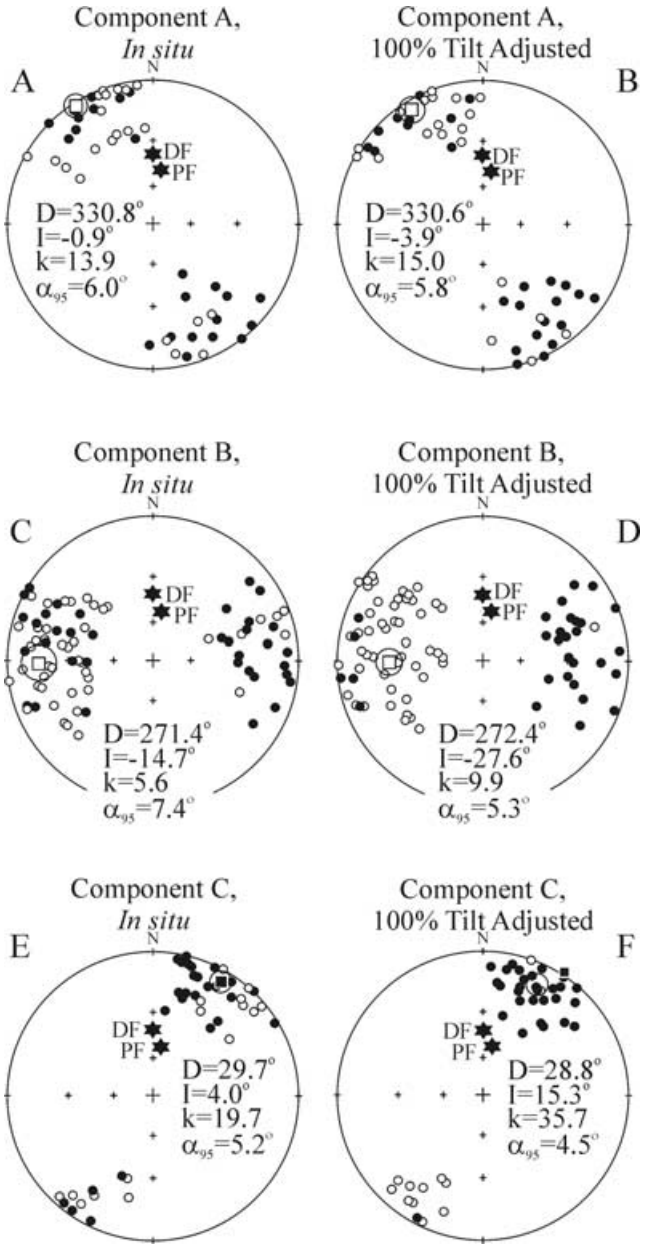

Figure 5. Site mean directions for components A, B and C displaying both *in situ* and tilt corrected data sets. In each of the figures, stars represent locations of the best-fitting dipole field (DF) and the present geomagnetic field (PF), respectively, expected in the sampling region. Stereonet is an equal are projection in which closed/open shapes denote reverse/normal polarities. Additionally, site mean directions are shown by open/closed squares for sites with normal/reverse characteristic directions with the associated uncertainty for each calculation.

the 42 sites in which component C was identified, with the remaining 13 contributing only slightly to the overall statistical outcome.

As the eastern-most Georgina Basin was not subject to folding until the Middle Carboniferous (Haines *et al.* 2001), tilt-adjusted data were used to determine site-level virtual geomagnetic poles (VGPs). This is compatible with the presence of component A magnetizations having partially overprinted C ChRMs (Fig. 3h). As both A and C have positive fold test results and A is generally less stable than C, it seems likely that C pre-dates A and tilt-adjusted data should, therefore, be used. It is proposed that the preservation of this remanence through basin inversion, multiple episodes of faulting, Carboniferous folding and uplift, and sustained Tertiary weathering is most likely the result of its commonly being found in dark grey limestones and reddish grey marls, lithologies that are typified, via 3-D IRM and palaeomagnetic analysis, by geologically stable remanence carriers.

The mean palaeopole for component C magnetizations, calculated from 41 VGPs, lies at $\lambda = 48.6°$N, $\phi = 186.0°$E, ($dp = 2.1°$, $dm = 4.0°$) (Table 3) and lies between the ∼490 Ma Black Hill Norite (BHN) pole of Schmidt *et al.* (1993) and the ∼530 Ma Todd River Dolomite (TOD) pole of Kirschvink (1978), agreeing with the Middle–Late Cambrian (∼510 Ma) age assigned to these carbonates (GBL in Fig. 8). The position of this pole on Australia's APWP, the positive outcomes of both reversal and fold tests, well-behaved rock magnetic results (Figs 2e, h, i), the observed (characteristic) linear decay of this component in orthogonal vector diagrams, and its dissimilarity to any younger segments of the Gondwanan APWP all support a primary origin for this magnetization.

4.3 The cluster analysis

Examination of the data presented in Table 2 and Fig. 5 reveals a certain amount of overlap between the more peripheral members of magnetizations assigned to the A, B and C components. When this occurred, discrimination between components was often based upon demagnetization behaviour. For example, when choosing between component B directions (E–W) and component A directions (NW–SE), ChRMs with lower unblocking temperatures and MDFs were assigned to the component B group directions. Likewise, in the few cases in which a sample (or site) could be grouped with either component B or the Cambrian direction (component C), those with higher unblocking temperatures and MDFs were grouped with the C component.

As a statistical check, a clustering algorithm (McFadden 1998) was applied to the entire ChRM data set. The outcome of this test

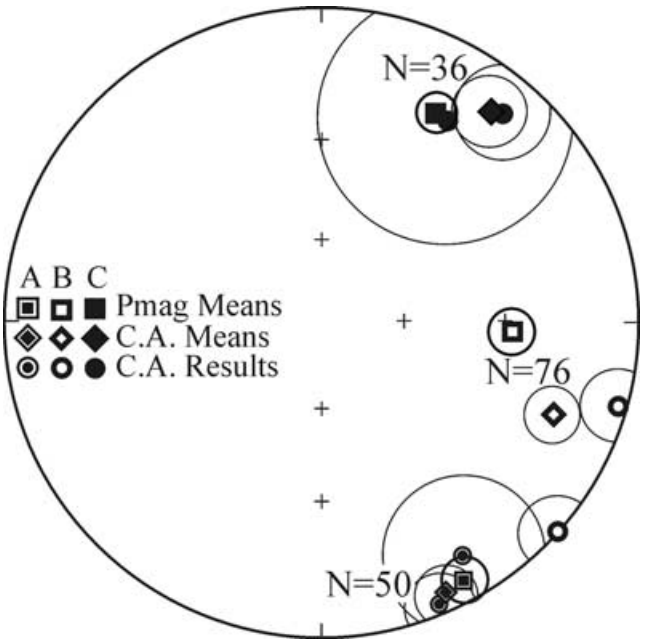

Figure 6. Cluster analysis (CA) results (McFadden 1998) of the three magnetization components described herein. N next to each clustering mean denotes the number of samples included in analysis. Stereonet is an equal area projection in which closed/open shapes denote reverse/normal polarities.

is shown in Fig. 6. Tight grouping of components similar to the A and C directions were identified using the clustering algorithm of McFadden (1998) and, at the 95 per cent confidence interval, the mean from each of the two clustering outputs cannot be distinguished from the respective means computed from isolated palaeomagnetic directions. Results thought to be related to B component directions are more problematic, as can be seen. Although each of the clustering algorithm results for the B components has a small associated uncertainty, the dispersion of the results is high. It is also evident from Fig. 6 that substantial overlap is present between the A and B components and it is recognized that the potential for bias in either or both of the mean directions computed for these ChRMs is high. These findings are consistent with the earlier claim of difficulty in isolating this ChRM due to extremely weak magnetizations and a probable inability to fully remove competing magnetization spectra.

5 DISCUSSION

5.1 Comparison with earlier investigation

As with the earlier study (Ripperdan & Kirschvink 1992), referred to, for the sake of brevity, as the R&K study for the remaining discussion, three Palaeozoic remanences were isolated in sampled Cambrian–Ordovician units. The overlap between components, detailed above, is also consistent with groupings identified with the earlier study, even if our interpretations are not in agreement. A summary table of both data sets, with *in situ* and tilt-corrected directions, is presented in Table 3 for comparison.

Component A from this study is indistinguishable at the 95 per cent confidence interval from the OVP^2 direction of that presented in the R&K study. In both studies, this direction is interpreted as an Early Devonian magnetization. Ripperdan & Kirschvink (1992) suggested the OVP^2 was most likely the result of fluid migration related to the early stages of the development of the Alice Springs Orogeny (ASO) of central Australia. The first phase of this intracratonic orogeny during the Early–Middle Devonian gave rise to thrust faulting of the Toko Syncline (Scheibner & Veevers 2000) and fluid migration during this period would be expected. This direction is constrained by a positive fold test and a positive reversal test for 100 per cent tilt-adjusted data. Folding within the eastern Georgina Basin is associated with a second pulse of ASO deformation during the Middle Carboniferous, an age assignment supported by horizontal Permian sediments overlying folded Carboniferous strata (Haines *et al.* 2001) and apatite fission track thermochronology within the Mt Isa Block (Spikings *et al.* 1997). Modelling of apatite fission track data from the Mt Isa Block shows vertical displacement of the region on the order of 0.06–0.3 km Myr^{-1} during the Carboniferous related to regional uplift and tectonic activity associated with the ASO (Spikings *et al.* 1997).

A comparison of component B directions with the CO1° direction of the R&K study (Table 3) reveals that although similarly directed, these magnetizations are dissimilar at the 95 per cent confidence interval; mean directions are separated by 32°. Component B directions have shallow to moderate negative inclinations while the CO1° direction is very shallow with a positive inclination. The reason for this discrepancy is unclear as a comparison of the direction acquired from the section sampled at Mt Unbunmaroo (Black Mountain) during this investigation (Table 3) is also dissimilar from that reported by the R&K study, contrary to what one might expect. One possible explanation for this inconsistency is that, assuming the B/CO1° directions are roughly analogous, this magnetization 'component' represents a more complex magnetization, perhaps somewhat obscured by the failure to fully remove other contributing magnetization components, as is suggested by the palaeomagnetic data in Figs 3c–e .

Similarity in the demagnetization behaviour between the B component magnetizations typified by univectorial decay on orthogonal projections (Fig. 3f) and those from the TR component, also suggests this remanence may have arisen from prolonged weathering related to Late Ordovician–Early Silurian basin inversion (Haines *et al.* 2001; Mawby *et al.* 1999). As detailed rock magnetic tests were not performed by the R&K study, were only marginally effective in isolating magnetic mineralogies during this investigation and AMS studies proved unfeasible, it seems unlikely that this ambiguity can be resolved.

Component C, which is interpreted herein as a primary Cambrian magnetization, is slightly steeper with more easterly directions than the OVP^1 direction of the R&K study (Table 3). Although indistinguishable at the 95 per cent confidence interval, the C and OVP^1 directions are subtended by 12.1°. The small difference between these two components may arise from contamination of the OVP^1 component with OVP^2 (NW) directions in the R&K study. In addition, the OVP^1 direction was described as having only south directions, whereas the results presented herein are of dual polarity, directed to the northeast–southwest.

Ripperdan & Kirschvink (1992) stated that the OVP^1 direction was 'particularly common around the contact between the Chatsworth Limestone and the Ninmaroo Formations' but attributed this magnetization to fluid migration in the Early Silurian. Component C is similarly found near the contact of these two formations, but is also common in underlying members of the Late Cambrian Chatsworth and Devoncourt Limestones. This component is not seen in Ordovician members of the Ninmaroo Formation, contributing to the arguments outlined above for a Late Cambrian primary or early diagenetic remanence for component C.

Magnetostratigraphic correlation between the Mt Unbunmaroo (Black Mountain) section and a similarly aged section from Dayangcha, China (Ripperdan *et al.* 1993), was presented in the R&K study and lent support to their definition of the CO1° direction as a primary magnetization. The differences in interpretation between the two Georgina Basin studies, therefore, merits a critical discussion related to the magnetostratigraphy in the R&K study.

Fig. 7 presents a magnetostratigraphic comparison between the CO1° direction from the R&K study and our B component. In this figure, we have compiled a magnetostratigraphic column of the B component utilizing both the conventional polarity (CP) option and the alternate polarity (AP) assignment. Although our preferred interpretation for B is it is a Silurian remagnetization, this is the component that R&K interpret as primary and, as such, should yield a similar magnetostratigraphic column irrespective of sampling section. The section we sampled can be accurately tied to the section sampled by R&K and, consequently, we are able to make a meaningful stratigraphic comparison between CO1° and B magnetozones. Nevertheless, as shown in Fig. 7, we find the correlation of magnetozones unconvincing. This is not surprising since the number of degrees of freedom in the comparison is of about the same order as the number of magnetozones.

Quality criteria for magnetostratigraphic studies are similar to those for palaeomagnetic investigations (Van der Voo 1990) and were formalized by Opdyke & Channell (1996). On examination of Ripperdan & Kirschvink's (1992) magnetostratigraphic data, 7 of the 10 Opdyke & Channell (1996) reliability criteria are met, and thus this study is apparently of high quality. However, we also make

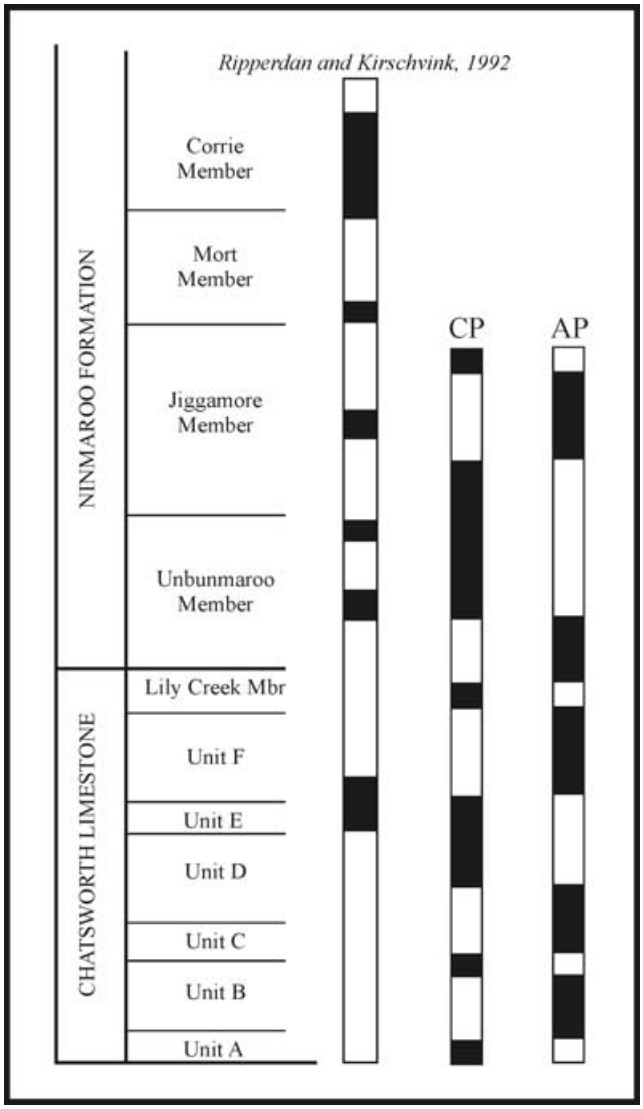

Figure 7. Magnetostratigraphic comparison between the CO1° direction from the R&K study and our B component. In this figure, we have compiled a magnetostratigraphic column of the B component utilizing both the conventional polarity (CP) option and the alternate polarity (AP) assignment.

the following observations regarding the R&K study that raises our concern that the magnetostratigraphic evidence is not unassailable.

First, results from Black Mountain by Ripperdan & Kirschvink (1992) are based upon a single section, with magnetozones at times defined by a single specimen, they lack field tests that would constrain relative magnetization ages, and from an original 140 samples only 66 samples yielded components that could be analysed using PCA. The remaining 7 magnetozones were defined by 'endpoints of two-component demagnetization trajectories' making it unclear whether stable endpoint directions were isolated. Also, assuming a time interval of some 20 Myr for this sequence, 70 samples represents approximately one sample per 300 kyr, if evenly spaced. Tauxe & Gallet (1991) have shown that random sampling of polarity over such time periods does not necessarily produce a self-consistent polarity history, necessitating multiple sections in the production of a reliable record. Furthermore, the very shallow inclinations reported for the CO1° direction in the R&K study ($I_{\text{mean}} = 4.3°$) make polarity assignment tenuous, at best. Finally, correlations between the Black Mountain and Dayangcha, China (Ripperdan *et al.* 1993) sections are problematic, as analysis of the results from the Dayangcha, China section, with respect to the magnetostratigraphic quality criteria, is hampered by the lack of published information.

Conodont and chemostratigraphic studies were not carried out during this investigation, precluding detailed correlation between the three sampling regions within the eastern Georgina Basin. As the C component was not isolated in each sampled bed, generation of a magnetostratigraphic column based on the available data would not be definitive and is not justified.

5.2 The revised APWP

The APWP presented in Fig. 8 invokes the 'alternate' polarity option, after Schmidt & Morris (1977), for pre-Devonian palaeopoles. Both the Morel & Irving (1978), utilized in the R&K study, and the Schmidt & Morris (1977) APWP models assume an autochthonous relation between cratonic Australia and elements comprising the Palaeozoic Tasman Fold Belt; the former, however, requires exceptionally fast plate velocities ($\geq$60 cm yr^{-1}) for Gondwana during the Early Palaeozoic, rates which are difficult to reconcile. By invoking 'alternate' polarities for poles older than ~400 Ma, plate velocities are slowed to some 15–25 cm yr^{-1}. All palaeopoles used in the generation of the APWP presented in Fig. 8 are listed in Table 4. Rotation of Gondwanan data into the Australian reference frame was accomplished using the rotation parameters of Lawver & Scotese (1987). The dgb (component A) and OVP[2] magnetizations plot slightly north and west of the Early Devonian Snowy River Volcanics (SRV) (Schmidt *et al.* 1987) and that of the Devonian aged dykes related to the Ravenswood Batholith (Clark 1996), DD in Fig. 8. The dgb palaeopole is thought to reflect a remagnetization acquired during the early stages of deformation related to thrust faulting of the Toko Syncline in the Georgina Basin during the Early–Middle Devonian (Haines *et al.* 2001). Folding of these strata most likely occurred during the second pulse (Middle Carboniferous) of the Middle Palaeozoic Alice Springs Orogeny (e.g. Haines *et al.* 2001; Spikings *et al.* 1997).

Ripperdan & Kirschvink (1992) considered the CO1° direction to reflect a primary Cambrian–Ordovician magnetization, based partially on the location of the CO1° pole on the Australian Palaeozoic APWP of Morel & Irving (1978) and in part upon their interpretation of the magnetostratigraphic column generated from CO1° magnetizations, discussed above. In the APWP presented in Fig. 8, the age attributed to component B/CO1° directions, poles sgb and CO1°, respectively, is ~430 Ma. As the sgb and CO1° palaeopoles fall near the well-defined series of ~420 Ma poles obtained from the Ravenswood Batholith and related dykes (Clark & Lackie 2003) and that of the Mereenie Sandstone (Li *et al.* 1991), and for the reasons outlined in the preceding discussion, we favour an Early Silurian remagnetization age for the sgb and CO1° directions.

The palaeopole calculated from component C, GBL in Fig. 8, falls upon the Cambrian loop, between the ~490 Ma Black Hill Norite (BHN) (Schmidt *et al.* 1993) and the ~530 Ma Todd River Dolomite (TOD) (Kirschvink 1978), in accordance with a Late Cambrian remanence age. Although the number of Cambrian palaeopoles from outside Australia is limited, the detailed inset in Fig. 8 presents a comparison between cratonic Australian data with palaeopoles from other Gondwanan continents and provides a persuasive basis for the primary Late Cambrian remanence attributed to GBL. In particular, the GBL pole is concordant with a series of Late Cambrian poles provided by Klootwijk (1980) from cratonic Australia, including the

Table 4. Palaeopoles used in the APWP presented in Fig. 8. Formation describes the rock unit from which the presented data were derived (all data are from Australia, unless otherwise noted); Mnemonic refers to the palaeopole designators in Fig. 8, Plat (°N)/Plong (°E) mark the location of the reported palaeopole in Australian coordinates; α_{95} is the half-angle of the 95 per cent circle of confidence associated with each mean direction; Age of magnetization refers to the presumed age of remanence in Ma; Q describes the palaeopole in terms of the quality criteria of Van der Voo (1990) and are not presented for remagnetizations; GPMDB Ref. No. corresponds to the reference number given in the Global Palaeomagnetic Database of McElhinny & Lock (1996) (now maintained by Sergei Pisarevsky at the Tectonics Special Research Centre, University of Western Australia and available on-line at http://www.geodynamics.no/). Lower case mnemonics refer to palaeopoles that are thought to reflect remagnetizations. Italicized entries are data presented from this study. Note that palaeomagnetic poles from the study carried out by Ripperdan & Kirschvink (1992) have been included in this table, with a reinterpretation of the age of magnetization attributed to their CO1° and OVP[1] poles, and are marked by (R&K) following the formation description. Gondwanan data have been rotated into the Australian reference frame using the rotation parameters of Lawver & Scotese (1987).

Formation	Mnemonic	Plat (°N)	Plong (°E)	α_{95}(°)	Age of magnetization (Ma)	Q	GPMDB Ref. no.
Devonian Dykes, Mt Leyshon	DD	−78.0	198.8	7.6	382–415	6	3262
Snowy River Volcanics	SRV	−74.3	222.7	9.7	391–417	7	1365
Georgina Basin, Devonian overprint	*dgb*	−54.7	262.3	4.5	390 − 410	*	*this study*
Georgina Basin, Devonian overprint (R&K)	ovp[2]	−61.2	254.1	15.5	390–420	*	3082
Silurian Dykes, Mt Leyshon	SD	−21.7	231.9	8.3	422–428	7	3262
Ravenswood Batholith	RVB	−17.5	232.7	7.1	422–428	7	3262
Mereenie Sandstone	MS	−15.7	242.7	25.6	417–443	5	2574
Hugh River Shale, overprint	hrs	−11.0	217.0	9.0	420–440	*	210
Stairway Sandstone, overprint	ss	2.0	230.5	10.0	420–440	*	192
Georgina Basin, Silurian overprint	*sgb*	−8.0	216.8	5.3	420–440	*	*this study*
Georgina Basin, Silurian overprint (R&K)	co1°	−3.1	234.1	7.4	420–440	*	3082
Jinduckin Formation	JF	13.0	205.0	13.0	485–490	4	202
Tasmanian Sediments	TS	19.4	208.9	10.4	490–505	5	3155
Black Hill Norite	BHN	37.5	214.4	3.8	485–495	5	2971
Sör Rondane Intrusions, Antarctica	SRI	28.5	189.5	4.5	485–495	3	546
Lake Frome Group	LLFG	31.4	206.9	10.1	505–515	3	1769
Purple Sandstone, Pakistan	PS	36.0	223.5	12.0	505–510	3	577
Carion Granite, Madagascar	GC	35.7	189.0	11.0	505–515	5	3405
Salt Pseudomorth Beds, Pakistan	SPB	26.6	213.5	5.9	505–515	4	209
Aroona Dam Sediments	ADS	36.0	213.0	16.5	505–525	3	206
Billy Creek Formation	BCF	37.4	200.1	14.4	510–520	5	1769
Kangaroo Island Sediments	KIS	33.8	195.1	12.3	515–525	5	1769
Pertaoorta Group	PG	32.7	191.5	7.3	505–545	6	1769
Georgina Basin Limestones	*GBL*	48.6	186.0	4.5	*∼510*	*7*	*this study*
Chatsworth Lmst/Ninmaroo Fm (R&K)	OVP[1]	57.2	179.3	11.4	∼ 510	5	3082
Giles Creek Dolomite	GCD	38.3	204.5	10.4	505–515	6	1769
Khewra Sandstone, Pakistan	KS	36.0	223.5	8.0	515–545	3	1412
Rewa Sandstones, India	RS	47.2	174.9	13.7	Cambrian	3	254
Jutana Formation, Pakistan	JFP	20.5	231.0	11.0	515–525	4	1412
Upper Arumbera Sandstone	AU	46.6	157.3	4.1	520–540	7	1070
Todd River Dolomite	TOD	43.2	159.9	6.7	525–535	7	1070
Bhandar and Rewa Series, India	BRS	43.3	152.4	11.1	Cambrian	3	1084
Upper Bhandar Sandstone, India	UBS	40.8	156.2	5.5	Cambrian	4	212
Bunyeroo Formation	BF	18.1	196.3	10.7	580–600	6	3099
Elatina Formation	EF	54.3	146.9	1.8	600–620	6	2463

Pertaoorta Group (PG), Giles Creek Dolomite (GCD), Billy Creek Formation (BCF), and that from the Kangaroo Island Sediments (KIS) (Fig. 8, inset). As these poles are spread throughout cratonic Australia, it is extremely unlikely that this agreement arises from localized rotations that have, fortuitously, resulted in a high level of conformity.

6 CONCLUSIONS

Two Cenozoic magnetizations are present within the eastern Georgina Basin: PF and TR. Whilst these directions do not impact the Palaeozoic findings, they are notable for the precision with which they have recorded recent directions of the Earth's magnetic field. Of the 350 or more samples for which NRM directions and intensities were measured, 202 provided an accurate reflection of the Earth's present field direction recorded by goethite. The TR component, likewise, provides a reliable estimate of the Earth's Tertiary magnetic field, a period of deep weathering across much of Australia, supporting the use of palaeomagnetism in the dating of prolonged weathering events through time (Schmidt & Embleton 1976).

An Early Devonian magnetization, component A, is constrained by positive results for fold and reversal tests. The associated palaeopole (dab) lies at $\lambda = 54.7°$S, $\phi = 262.3°$E ($N = 46$, $dp = 2.3°$, $dm = 4.5°$). This direction is thought to be related to fluid migration in the Early Devonian arising from large-scale thrust faulting within the Georgina Basin that placed the southwestern margin of the Toko Syncline beneath the Proterozoic Arunta Inlier (Haines *et al.* 2001).

The sgb pole, $\lambda = 8.0°$S, $\phi = 216.8$E° ($N = 77$, $dp = 2.6°$, $dm = 5.1°$), is thought to be analogous to the CO1° pole of Ripperdan

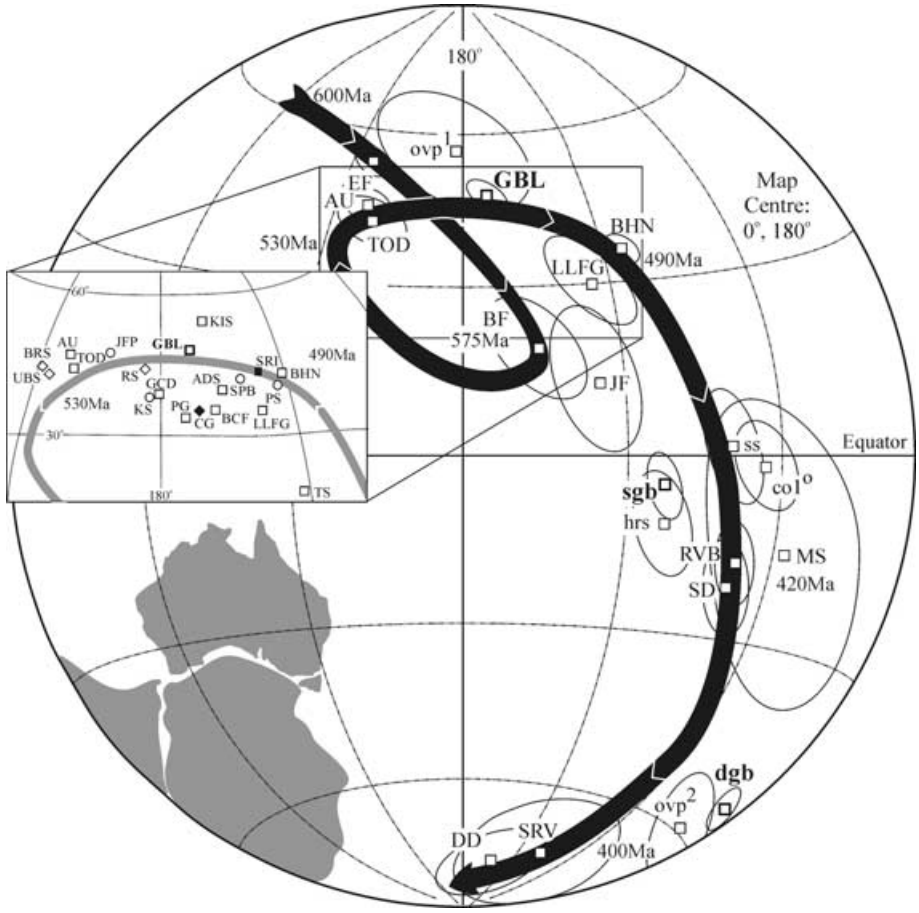

Figure 8. Revised Early Palaeozoic APWP for Australia. Palaeomagnetic poles used in the construction of Fig. 8 are listed in Table 4. Lower case mnemonics refer to palaeopoles that are thought to reflect remagnetizations. Palaeozoic palaeopoles that are associated with this study are marked by bold print. Palaeopoles coming from previously published Australian data are marked by open squares. Palaeopoles shown in the Cambrian aged insert are from Australia (open squares), Madagascar (filled diamond), India (open diamond), Antarctica (filled square) and Pakistan (open circles). Gondwana and constituent data have been rotated into the Australian reference frame using the rotation parameters of Lawyer & Scotese (1987). Plot is an equal area projection with map centre located at 0°, 180°E generated with GMAP-32 (Torsvik & Smethurst, 1989–1997).

& Kirschvink (1992). The CO1° direction of the R&K study was cited as a fundamental palaeopole in the proposed Middle–Late Cambrian IITWP event (Kirschvink *et al.* 1997) and the data presented herein provide a reinterpretation of palaeomagnetic data from Mt Unbunmaroo and surrounding areas that do not support a Late Cambrian–Early Ordovician age for this remanence, but rather a remagnetization related to documented Late Ordovician–Early Silurian deformation. Basin inversion led to the disruption of the Late Proterozoic–Early Palaeozoic Larapitine Seaway, bringing to an end the long-lived carbonate deposition within the basin (Scheibner & Veevers 2000). This flexural event could have been accompanied by fluid migration or sustained weathering of newly exposed strata, allowing for growth of new magnetic mineralogies. Results from applied clustering algorithm analysis, reversal tests and fold tests were inconclusive, making a claim for primary origin of this remanence difficult to substantiate.

An arguably primary, or early diagenetic, remanence direction was isolated in the Cambrian Chatsworth and Devoncourt Limestones and within Cambrian members of the Ninmaroo Formation. This palaeopole, GBL, lies at $\lambda = 48.6°$N, $\phi = 186.0°$E ($N = 42$, $dp = 2.1°$, $dm = 4.0°$), has positive reversal test and fold test statistics and provides for a high degree of conformity within the greater Gondwanan data set.

Debate continues surrounding the proposed Cambrian IITPW event of Kirschvink *et al.* (1997) (e.g. Evans 1998; Meert 1999; Torsvik & Rehnström 2001; Torsvik *et al.* 1998). Since the initial proposal, new geochronological data have become available that place strict limitations on the duration of this event (Davidek *et al.* 1998; Landing *et al.* 1998). While the paucity of high-quality Cambrian palaeomagnetic data allows for various interpretations of the available data set, recent palaeomagnetic studies provide tight constraints on the magnitude of continental drift velocities during this period (McCausland & Hodych 1998; Pisarevsky *et al.* 1998; Smethurst *et al.* 1998) and new results from the region surrounding Mt Unbunmaroo (Black Mountain) have important ramifications upon this debate.

The ∼510 Ma remanence age attributed to the GBL palaeopole places it within the younger boundary of the proposed IITPW event (Evans 2003, Meert 1999). Kirschvink *et al.* (1997) chose the ∼530 Ma Tod River Dolomite (TOD) (Kirschvink 1978) palaeopole as a marker pole for the palaeomagnetic data set defining Australia's APWP prior to the onset of the IITPW event. The angular separation between the GBL palaeopole (which is conformable with a series of Late Cambrian poles from cratonic Australian presented by Klootwijk (1980)) and the TOD palaeopole is only 18.8°, translating into a drift velocity of ∼10 cm y^{-1}. These values fall far short

of the 90° rotation and the drift rates of more than 60 cm yr^{-1} for Early Palaeozoic continental blocks demanded by IITPW in any of its incarnations.

ACKNOWLEDGMENTS

We thank Joe Meert and Joe Kirschvink for their critical and extremely beneficial reviews of this work and Cor Langereis in his role as *GJI* Editor. Discussions related to the contributions of these three have resulted in a greatly improved manuscript. We would also like to thank Valerian Bachtadse, Dennis Kent and Zheng-Xiang Li for reviews of early versions of this manuscript; the CSIRO for supporting this project; John Draper and Simon Crouch of the Queensland Department of Mines and Energy for information related to the geological evolution of the southern Georgina Basin; Dr Glenn Brock of MUCEP for assistance in setting up field trips to this area; Peter Malloy of MUCEP for his time and assistance in dissolving specimens for rock magnetic tests; Mark Huddleston, Gene Justice and Ché Anderson Justice for invaluable assistance in the field; and the station owners around Boulia, QLD, for allowing access to paddocks and tracks and priceless advice on how to find the way up the mountains. This work was supported in part by a Sigma Xi Grant in Aid of Research, a Macquarie University Post-graduate Research Award, and CSIRO. This is contribution 323 from the ARC National Key Centre for Geochemical Evolution and Metallogeny of Continents (GEMOC).

REFERENCES

Clark, D.A. & Lackie, M.A., 2003. Palaeomagnetism of the Early Permian Mount Leyshon Intrusive Complex and Tuckers Igneous Complex, north Queensland, Australia, *Geophys. J. Int.,* **153,** 523–547.

Davidek, K., Landing, E., Bowring, S.A., Westrop, S.R., Rushton, A.W.A., Fortey, R. & Adrain, J.M., 1998. New uppermost Cambrian U–Pb date from Avalonian Wales and the age of the Cambrian–Ordovician boundary, *Can. J. Earth Sci.,* **35,** 303–309.

Dunlop, D.J. & Özdemir, Ö., 1997. *Rock Magnetism: Fundamentals and Frontiers,* Cambridge University Press, Cambridge, p. 573.

Evans, D.A., 1998. True polar wander, a supercontinental legacy, *Earth planet. Sci. Lett.,* **157,** 1–8.

Evans, D.A.D., 2003. True polar wander and supercontinents, *Tectonophysics,* **362,** 303–320.

Fisher, R.A., 1953. Dispersion on a sphere, *Proc. R. Soc. London, Ser. A,* **217,** 295–305.

Haines, P.W., Hand, M. & Sandiford, M., 2001. Palaeozoic synorogenic sedimentation in central and northern Australia: a review of distribution and timing with applications for the evolution of intracontinental orogens, *Aust. J. Earth Sci.,* **48,** 911–928.

Kirschvink, J.L, 1978. The Precambrian-Cambrian boundary problem: paleomagnetic directions from the Amadeus Basin, Central Australia, *Earth planet. Sci. Lett.,* **40,** 91–100.

Kirschvink, J.L., 1980. The least-squares line and plane and the analysis of palaeomagnetic data, *Geophys. J. R. astr. Soc.,* **62** ,699–718.

Kirschvink, J.L., Ripperdan, R.L., & Evans, D.A., 1997. Evidence for large-scale reorganization of Early Cambrian continental masses by inertial interchange true polar wander, *Science,* **277,** 541–545.

Klootwijk, C.T., 1980. Early Palaeozoic palaeomagnetism in Australia, *Tectonophysics,* **64,** 249–332.

Landing, E., Bowring, S.A., Davidek, K.L., Westrop, S.R., Geyer, G. & Heldmaier, W., 1998. Duration of the Early Cambrian: U-Pb ages of volcanic ashes from Avalon and Gondwana, *Can. J. Earth Sci.,* **35,** 329–338.

Lawver, L.A. & Scotese, C.R., 1987. A revised reconstruction of Gondwanaland, in, *Gondwana Six; Structure, Tectonics, and Geophysics,* ed. McKenzie, G.D., pp. 17–23, American Geophysical Union, Washington, DC.

Li, Z.X., Powell, C.McA., Embleton, B.J.J. & Schmidt, P.W., 1991. New palaeomagnetic results from the Amadeus Basin and their implications for stratigraphy and tectonics, *Aust. Bur. Min. Res. Bul.,* **236,** 349–360.

Lodwick, W.R. & Lindsay, J.F., 1990. Southern Georgina Basin: a new perspective, *APEA J.,* **30,** 137–148.

Lowrie, W., 1990. Identification of ferromagnetic minerals in a rock by coercivity and unblocking temperature properties, *Geophys. Res. Lett.,* **17,** 159–162.

Mawby, J., Hand, M. & Foden, J., 1999. Sm-Nd evidence for high-grade Ordovician metamorphism in the Arunta Block, central Australia, *J. Met. Geol.,* **17,** 653–668.

McCausland, P.J.A. & Hodych, J.P., 1998. Paleomagnetism of the 550 Ma Skinner Cove volcanics of western Newfoundland and the opening of the Iapetus Ocean, *Earth planet. Sci. Lett.,* **163,** 15–29.

McElhinny, M.W. & Lock, J., 1996. IAGA paleomagnetic data bases with access, *Surv. Geophys.,* **17,** 575–591.

McElhinny, M.W., Powell, C.McA. & Pisarevsky, S.A., 2003. Paleozoic terranes of eastern Australia and the drift history of Gondwana, *Tectonophysics,* **362,** 41–65.

McFadden, P.L., 1998. The fold test as an analytical tool, *Geophys. J. Int.,* **135,** 329–338.

McFadden, P.L. & Jones, D.L., 1981. The fold test in palaeomagnetism, *Geophys. J. R. astr. Soc.,*

McFadden, P.L. & Lowes, F.J., 1981. The discrimination of mean directions drawn from a Fisher distribution, *Geophys. J. R. astr. Soc.,*.**67,** 19–33. **67,** 53–58.

Meert, J.G., 1999. A paleomagnetic analysis of Cambrian true polar wander, *Earth planet. Sci. Lett.,* **168,** 131–144.

Morel, P. & Irving, E., 1978. Tentative palaeocontinental maps for the Early Phanerozoic and Proterozoic, *J. Geol.,* **86,** 535–561.

Mound, J.E., Mitrovica, J.X., Evans, D.A. & Kirschvink, J.L., 1999. A sea-level test for inertial interchange true polar wander, *Geophys. J. Int.,* **136,** F5–F10.

Narbonne, G.M, Kaufman, A.J. & Knoll, A.H., 1994. Integrated chemostratigraphy and biostratigraphy of the Windermere Supergroup, northwestern Canada; implications for Neoproterozoic correlations and the early evolution of animals, *Geol. Soc. Am. Bull.,* **106,** 1281–1292.

Opdyke, N. & Channell, J., 1996. *Magnetic Stratigraphy,* Academic Press, London.

Pisarevsky, S.A., Gurevich, E.L. & Khramov, A.N., 1997. Paleomagnetism of Lower Cambrian sediments from the Olenek River section (northern Siberia): palaeopoles and the problem of magnetic polarity in the Early Cambrian, *Geophys. J. Int.,* **130,** 15–29.

Radke, B.M., 1982. Late diagenetic history of the Ninmaroo Formation (Cambro-Ordovician), Georgina Basin, Queensland and Northern Territories, *BMR J. Aust. Geol. Geophys.,* **7,** 231–254.

Ripperdan, R.L. & Kirschvink, J.L., 1992. Paleomagnetic results from the Cambrian-Ordovician boundary section at Black Mountain, Georgina Basin, western Queensland, Australia, in *Global perspectives on Orodovician geology,* pp. 93–103, ed. Webby, B.D., Laurie, J.R. & Balkema, A.A., Rotterdam, the Netherlands.

Ripperdan, R.L., Magaritz, M. & Kirschvink, J.L., 1993. Carbon isotope and magnetic polarity evidence for non-depositional events within the Cambrian-Ordovician Boundary section near Dayangcha, Jilin Province, China, *Geol. Mag.,* **130,** 443–452.

Schmidt, P.W. & Embleton, B.J.J., 1976. Palaeomagnetic results from sediments of the Perth Basin, Western Australia, and their bearing on the timing of regional lateritisation, *Palaeogeogr. Palaeoclimatol. Palaeoecol.,* **19,** 257–273.

Schmidt, P.W. & Morris, W.A., 1977. An alternative view of the Gondwana Paleozoic apparent polar wander path, *Can. J. Earth Sci.,* **14,** 2674–2678.

Schmidt, P.W., Clark, D.A. & Rajagopalan, S., 1993. An historical perspective of the Early Palaeozoic APWP of Gondwana: New results from the Early Ordovician Black Hill Norite, South Australia, *Expl. Geophys.,* **24,** 257–262.

Schmidt, P.W., Embleton, B.J.J. & Palmer, H.C., 1987. Pre and post folding magnetization from the Devonian Snowy River Volcanics and Buchan Caves Limestone, Victoria, *Geophys. J. R. astr. Soc.,* **91,** 155–170.

Scheibner, E. & Veevers, J.J., 2000. Tasman Fold Belt System, in *Billion-year Earth history of Australia and Neighbours in Gondwanaland,* pp. 154–233, ed. Veevers, J.J., GEMOC Press, Sydney.

Smethurst, M.A., Khramov, A.N. & Pisarevsky, S., 1998. Paleomagnetsim of the Lower Ordovician Orthoceras limestone, St. Petersburg, and a revised drift history for Baltica in the early Paleozoic, *Geophys. J. Int.,* **133,** 44–56.

Spikings, R.A., Foster, D.A., & Kohn, B.P., 1997. Phanerozoic denudation history of the Mt Isa inlier, northern Australia; response of a Proterozoic mobile belt to intraplate tectonics, *Int. Geol. Rev.,* **39,** 107–124.

Tauxe, L. & Gallet, Y., 1991. A jackknife for magnetostratigraphy, *J. geophys. Res.,* **18,** 1783–1786.

Torsvik, T.H. & Rehnström, E.F., 2001. Cambrian palaeomagnetic data from Baltica; implications for true polar wander and Cambrian palaeogeography, *J. geol. Soc. Lond.,* **158,** 321–329.

Torsvik, T. & Smethurst, M., 1989. *GMAP-32,*Geographic Mapping and Reconstruction System, Geol. Survey of Norway.

Torsvik, T.H. & Van der Voo, R., 2002. Refining Gondwana and Pangea palaeogeography: estimates of Phanerozoic non-dipole (octupole) fields, *Geophys. J. Int.,* **151,** 771–794.

Torsvik, T.H., Meert, J.G. & Smethurst, M.A., 1998. Polar wander and the Cambrian, *Science,* **279,** 9a.

Turner, S. & Young, G.C., 1987. Shark teeth from the Early—Middle Devonian Cravens Peak Beds, Georgina Basin, Queensland, *Alcheringa,* **11,** 233–244.

Van der Voo, R., 1990. The reliability of palaeomagnetic poles, *Tectonophysics,* **184,** 1–9.

Veevers, J.J., 2000. Present tectonic state, in, *Billion-year Earth history of Australia and Neighbours in Gondwanaland,* pp. 61–73, ed. Veevers, J.J., GEMOC Press, Sydney.

Zijderveld, J.D.A., 1967. A. C. demagnetization of rocks: analysis of results, in *Methods in Palaeomagnetism,* pp. 254–286, ed. Collinson, D.W., Creer, K.M. & Runcorn, S.K., Elsevier, New York.